FGF/ERK autocrine signaling is enhanced by NANOG in a subpopulation of pluripotent stem cells to execute autoregulation and induce heterogeneity

Hanuman T Kale, Rajendra Singh Rajpurohit, Debabrata Jana, Vishnu V Vijay, Mansi Srivastava, Preeti R Mourya, Gunda Srinivas, P Chandra Shekar*
CSIR-Centre for Cellular and Molecular Biology, Uppal Road, Hyderabad, Telangana, India 500007.
*Correspondence: csp@ccmb.res.in

SUMMARY:

FGF/ERK autocrine signaling induces *Nanog* heterogeneity, allelic switching, and differentiation in pluripotent cells, which are abolished in the naive-state (2i) by inhibition of MEK1/2 and GSK3β. Surprisingly *Nanog* autorepression is functional in 2i. The mechanisms activating FGF signaling and its downstream effectors leading to heterogeneity and allelic switching are unknown. We utilized genome-edited fluorescent reporter cell lines of both *Nanog* promotor and protein to elucidate, a NANOG induced FGF autocrine signaling mediated autoregulatory mechanism. We show that *Nanog* autoregulation is a cell non-autonomous process initiated by NANOG, but executed by FGF/ERK. FGFR2 differentially activates autoregulation in *Nanog*-high cells by activating ERK1/2. pERK1/2 recruits NONO (P54nrb) to repress *Nanog* transcription. Collectively, we show that *Nanog*-induced FGF autocrine signaling mediated autoregulation is the basis of *Nanog* heterogeneity and allelic switching. Our data introduces an unexpected reciprocal regulatory mechanism between NANOG and FGF/ERK signaling feeding into each other's heterogeneity.

INTRODUCTION

Embryonic stem (ES) cells are characterized by long-term self-renewal and the potential to differentiate to all cell types of the germ layers. ES cells cultured in presence of serum and LIF (metastable state) manifest transcriptional and functional heterogeneity. The heterogeneous

expression of transcription factors like *Nanog*, *Rex1*, *Stella*, *Esrrb*, *Klf4*, and *Tbx3* determine differential fate choice (Chambers et al., 2007; Festuccia et al., 2012; Filipczyk et al., 2013; Hayashi et al., 2008; Kalmar et al., 2009; Niwa et al., 2009; Torres-Padilla and Chambers, 2014; Toyooka et al., 2008; van den Berg et al., 2008). The molecular heterogeneity arising from the modulation of transcription factors by non-genetic factors underpins the functional heterogeneity of the subpopulations of ES cells. The core pluripotency factor, *Nanog* was identified as a factor conferring LIF independent self-renewal to ES cells by inhibiting differentiation (Chambers et al., 2003; Mitsui et al., 2003). *Nanog* imparts functional heterogeneity to ES cells through its heterogeneous expression leading to differential cell fate choices (Chambers et al., 2007; Kalmar et al., 2009). Unlike other core pluripotency factors, *Nanog* switches between mono-allelic and bi-allelic expression during embryonic development and in alternate pluripotency states (Filipczyk et al., 2013; Miyanari and Torres-Padilla, 2012). The expression of *Nanog* is restricted in ES cells to ensure their potential to differentiate by negative feedback autorepression and other repressive mechanisms (Fidalgo et al., 2012; Fidalgo et al., 2011; Mora-Castilla et al., 2010; Navarro et al., 2012; Pereira et al., 2006).

FGF/ERK signaling represses *Nanog* to induce heterogeneity and monoallelic expression, which are abolished in ESCs cultured in 2i (Filipczyk et al., 2013; Miyanari and Torres-Padilla, 2012). Intriguingly, *Nanog* autorepression is functional in 2i, suggesting MEK1/2 and GSK3β are dispensable for *Nanog* autoregulation (Navarro et al., 2012). Hence, the mechanisms regulating the three paradigms of *Nanog* regulation- heterogeneity, allelic expression, and autorepression are not entirely connected through FGF signaling. Although FGF/ERK represses *Nanog* expression (Hamazaki et al., 2006; Kim et al., 2014), the mechanistic delineation of this process is limited, and it is unclear how the NANOG protein levels are sensed by cells to trigger autorepression. Here, we utilized genetic approaches in *Nanog* fluorescent reporter cell lines and biochemical experiments to unravel a detailed mechanism of *Nanog* autoregulation. We show that MEK1/2 is essential for *Nanog* autoregulation. NANOG induces components of the FGF autocrine pathway in cells with higher *Nanog* expression, to trigger feedback repression by activation of ERK1/2. *Fgfr2* gene acts as a sensor of the NANOG protein in *Nanog* high cells. Further, we show that pERK1/2 interacts and recruits NONO to repress *Nanog* transcription. Surprisingly *Nanog* is essential only for triggering the autoregulation process but dispensable for its execution. Our results establish that the different facets of *Nanog* expression- heterogeneity, allelic switching, and autoregulation are regulated and interlinked by FGF autocrine signaling.

RESULTS

Residual MEK1/2 activity in the ground state prevents complete derepression of *Nanog*.

Nanog exhibits homogenous and biallelic expression in 2i. To uncouple the influence of MEK1/2 and GSK3β on *Nanog* expression, we analyzed the activity of endogenous *Nanog* gene activity reported by GFP in TNGA and TβC44Cre6 cell lines (Chambers et al., 2007) in different combinations of MEK1/2 and GSK3β inhibitors. *Nanog* promoter activity was derepressed in MEK1/2 inhibition (SLPD), GSK3β inhibition (SLCHIR), and 2i. Surprisingly *Nanog* promoter activity was higher in SLPD than in 2i (Figure1A, 1B). To analyze NANOG protein dynamics, we generated a NiRFP2A cell line with an iRFP670 coding sequence fused to the c-terminal of both alleles of *Nanog* (Figure S1A). Higher NANOGiRFP in SLPD (Figure1C, S1B), reaffirmed the highest induction of *Nanog* transcript and protein in SLPD. To dismiss the interference of any genetic modifications in the *Nanog* locus on its expression (Faddah et al., 2013); *Nanog* expression was analyzed in E14Tg2a cells. The *Nanog* transcript (Figure1D), transcriptional activity (Figure1E), and protein (Figure1F) were highest in SLPD. On the contrary, *Oct4* transcript and transcription activity were enhanced but protein changed very little in SLPD (Figure1D-F, S1C). NANOG was nearly 7-fold more in PD, which is twice that of 2i/SL2i (Figure1F). Although SLPD and 2i contain 1 μM PD, higher *Nanog* expression in SLPD indicates inefficient repression of *Nanog* in 2i/SL2i. We analyzed MEK1/2 substrate -pERK1/2 to investigate possible modulation of MEK1/2 activity by GSK3β (Yun et al., 2005). The pERK1/2 levels in ESCs changed dynamically throughout 24 hrs after the SL media was changed. The pERK1/2 remained undetectable up to 4 hrs in SLPD and 2i/SL2i. It gradually increased in 2i after 8 hrs but remained undetectable in SLPD (Figure 1G, S1D). We further analyzed pERK1/2 at different time points of treatment in PD, CHIR, and 2i/SL2i relative to SL after 24 hrs of media change (SL-24h). The pERK1/2 in SLCHIR and 2i significantly exceeded SL and SLPD respectively by 24 hrs (Figure 1H, S1E), suggesting a long-term CHIR treatment enhanced MEK1/2 activity in ESCs. Further, the PD and CHIR dose-responsive experiments confirmed that the pERK1/2 positively correlated with the CHIR concentrations (Figure 1I-J, S1F-I). Collectively, our data demonstrate that *Nanog* attains higher expression in MEK1/2 inhibition than in 2i. GSK3β activity negatively modulates MEK1/2 activity and its inhibition by CHIR increases pERK1/2

in 2i over time.

FGF autocrine signaling pathway components are essential for *Nanog* autoregulation.

The *Nanog* expression is higher in SLPD than 2i and *Nanog* autorepression is functional in 2i (Navarro et al., 2012). We asked if all repressive mechanisms including the *Nanog* autorepression are abolished in SLPD. To address this, we generated two independent NANOG restoration systems by integrating Flag-Avi-NANOG-ER^{T2} (NANOGER^{T2}) and a Doxycycline-inducible Flag-Avi-NANOG (FaNANOG) transgene in Tβc44Cre6 (Chambers et al., 2007) to derive the TNERT and TDiN cell lines respectively. TNERT and TDiN are similar to NERTc3 and 44iN (Festuccia et al., 2012; Navarro et al., 2012) where the NANOG function is reinstated by 4-Hydroxytamoxifen (OHT) or Doxycycline respectively, and endogenous *Nanog* gene activity is reported by GFP (Figure 2A, S2A-B). The repression of *Nanog*:GFP upon induction of transgenic NANOG by OHT/Dox is a functional readout of *Nanog* autoregulation. *Nanog*:GFP was repressed in OHT/Dox treated TNERT/TDiN in SL, SLCHIR, 2i, and SL2i, but not in SLPD (Figure 2A, S2C-D). To analyze the dynamics of endogenous NANOG in *Nanog* autoregulation, we generated NsGFPDiN cell line. The NANOG-GFP fusion protein is produced from one of the alleles of *Nanog* and a Doxycycline-inducible FaNANOG transgene is randomly inserted (Figure 2B). The NANOG-GFP was repressed in all treatments except in SLPD in Doxycycline treatment (Figure 2B, S2E). The data from distinct cell lines conclusively establish an essential role of MEK1/2 in *Nanog* autoregulation. We propose that the residual pERK1/2 resulting from residual MEK1/2 activity in 2i is sufficient for the functioning of *Nanog* autoregulation.

FGF autocrine signaling is the predominant inducer of MEK/ERK in pluripotent cells (Kunath et al., 2007; Lanner and Rossant, 2010), we investigated the role of FGF signaling components in autoregulation. NANOGER^{T2}/FaNANOG failed to repress *Nanog*:GFP in presence of FGFR inhibitor- SU5402, suggesting an essential role of FGFRs in *Nanog* autoregulation (Figure 2C, S2F). FGFR1, FGFR2, and FGF4 are major receptors and ligands of FGF signaling in early embryos respectively (Kang et al., 2017; Molotkov et al., 2017). FGFBP1 is a carrier protein expressed from early to late blastocyst (Figure 2D) (Park et al., 2015) that enhances FGF signaling (Tassi et al., 2001). We deleted *Fgfr1*, *Fgfr2*, *Fgf4*, and *Fgfbp1* in TNERT cells to analyze their role in autoregulation (Figure 2E, S2G-J). Except in

TNERTFgfr1-/-, *Nanog*:GFP was not repressed in TNERTFgfr2-/-, TNERTFgf4-/- and TNERTFgfbp1-/- cells upon OHT induction (Figure 2F). Our data suggest that FGF autocrine signaling and its components FGFR2, FGF4, and FGFBP1 are essential for *Nanog* autoregulation.

Nanog enhances the expression of FGF autocrine signaling pathway components.

We analyzed the expression of FGF autocrine signaling components during the time course of OHT induction. *Fgf4, Fgfr2, Fgfr1,* and *Fgfgbp1* transcripts were induced within 1-2 hrs (Figure 3A), *Esrrb* a direct target of NANOG was induced within 0.5 hrs. Increased pre-mRNA of *Fgf4, Fgfr2, Fgfbp1, and Fgfr1* indicated transcriptional activation of FGF signaling pathway components after OHT induction (Figure 3B). ChIP-seq data analysis identified NANOG occupancy on *Fgf4, Fgfbp1, Fgfr1,* and *Fgfr2,* which was further enhanced in *Oct4*+/- cells that have higher NANOG (Figure S3A) (Karwacki-Neisius et al., 2013). To analyze dosage-dependent occupancy of NANOG on these genes, we generated EDiN cell line by introducing a Doxycycline- inducible FaNANOG transgene in E14Tg2a. ChIP-PCR confirmed NANOG occupancy on *Fgf4, Fgfbp1, Fgfr1,* and *Fgfr2,* which was further enhanced in PD (Figure 3C) and EDiN+Dox (Figure 3D) which express higher NANOG. The data suggest a dose-dependent occupancy of NANOG on the FGF signaling component genes. FGFR1, FGFR2, and pERK1/2 were significantly increased upon OHT induction in TNERT (Figure 3E). The strength of FGF signaling depends on facilitation by carrier proteins (Tassi et al., 2001), the affinity of ligands (Ornitz et al., 1996; Zhang et al., 2006), and subsequent subcellular trafficking of the FGFRs after ligand-mediated activation (Auciello et al., 2013; Francavilla et al., 2013). The induction of NANOGER^{T2} enhanced FGFR2 on the cell surface (Figure 3F), unlike the FGFR1 (Figure S3B). The NANOGER^{T2} induction increased FGF4 and FGFBP1 secretion by TNERT (Figure 3G- H, S3C-D). Collectively the data shows that increased NANOG enhances FGFR2 on the cell surface, and secretion of FGF4 and FGFBP1 to intensify the FGF autocrine signaling. NANOG induces and enhances FGF autocrine signaling to execute *Nanog* autoregulation.

Nanog autoregulation is a cell non-autonomous process mediated by FGF autocrine/paracrine signaling.

Nanog autorepression is suggested to operate by a cell-autonomous process through intracellular proteins NANOG, ZFP281, and NURD complex (Fidalgo et al., 2012). However, Cell non-autonomous function of *Nanog* in the induction of primitive endoderm (Frankenberg et al., 2011; Messerschmidt and Kemler, 2010) and the essential role of secreted proteins FGF4 & FGFBP1 in autoregulation from our experiments prompted us to investigate cell non-autonomous mechanisms. We assessed the ability of conditioned media from OHT induced TNERT cells, to repress *Nanog*:GFP in T*β*c44Cre6 lacking Nanog (Figure 3I). The conditioned media was sufficient to repress the *Nanog*:GFP (Figure 3J, S3E), suggesting that autoregulation operates via cell non-autonomous mechanisms and discounts the direct role of NANOG in autorepression as proposed earlier (Fidalgo et al., 2012). NANOG seems to be essential for triggering autoregulation through FGF signaling components but does not participate in repression. This led us to investigate the role of ZFP281 in *Nanog* autoregulation. The repression of *Nanog:*GFP upon OHT treatment, in TNERTZfp281-/- cell line lacking Zfp281 (S3F) suggests that ZFP281 is dispensable for *Nanog* autoregulation (Figure 3K).

To evaluate if FGF4 secretion was the causative factor of *Nanog* autoregulation in the conditioned media, we treated T*β*c44Cre6 with conditioned media from cells with loss or gain of FGF4. The conditioned media from an E14Tg2a cell line overexpressing FGF4 or supplementation of FGF4 (50ng/ml) could repress *Nanog*:GFP. Conversely, the conditioned media from OHT induced TNERTFgf4-/- or from TNERT+OHT-0 hr cells failed to repress *Nanog*:GFP, suggesting FGF4 is the key secreted factor essential for *Nanog* autoregulation (Figure 3L, S3G). The ELISA analysis confirmed the secretion and accumulation of FGF4 and FGFBP1 in the conditioned media (S3H-K). Collectively, our data establish that *Nanog* autoregulation is a cell non-autonomous process triggered by NANOG by augmenting FGF autocrine/paracrine signaling.

NANOG-induced FGFR2 triggers autoregulation predominately in the ES cell population with higher *Nanog* expression.

Nanog autoregulation was proposed to restrict NANOG levels within limits to retain the differentiation potential (Fidalgo et al., 2012; Navarro et al., 2012). *Nanog* autoregulation is expected to operate only in *Nanog*-high cells and not in *Nanog*-low cells. To evaluate this logic, we used TDiN cell lines with different induction levels of FaNANOG (Figure S4A).

The strength of *Nanog* autoregulation was found to be dependent on the FaNANOG levels and was completely abolished in TDiN clone with low FaNANOG (Figure S4B, 4C). To analyze autoregulation in *Nanog*-high and *Nanog*- low cells, we sorted the lowest and the highest 10% population of the TNERT expressing GFP and treated with OHT. The *Nanog:*GFP was repressed in *Nanog*-high cells but not in *Nanog*-low cells (Figure 4A). Our experiments demonstrate the logic of *Nanog* autoregulation and conclude that *Nanog* autoregulation predominately operates in *Nanog*-high and not in *Nanog*-low cell population.

FGF4 and FGFBP1 are secretory proteins, hence cannot distinguish between the *Nanog*- high and low cells in culture. Whereas FGFRs are essential for autoregulation and are retained on the cells, we asked if FGFRs functioned as a sensor for the NANOG levels to distinguish *Nanog*-high cells from low cells. We analyzed the correlation between the expression of FGFR1 and FGFR2 vis-à-vis NANOG in E14Tg2a by FACS. FGFR2 and FGFR1 showed a strong correlation with NANOG, which was further enhanced for FGR2-NANOG in SLPD (r=0.80) whereas decreased for FGFR1-NANOG (r=0.59) in SLPD (Figure 4B,) where NANOG levels are higher. These data suggested FGFR2 but not FGFR1 expression levels correlate and respond to NANOG concentration in the cells. FACS analysis showed high FGFR2 in the 10% NANOG high population and lower FGFR2 in the 10% NANOG low population (Figure 4C). The dose-dependent binding of NANOG to *Fgfr2* and a strong FGFR2-NANOG correlation suggest that the *Fgfr2* gene may function as a sensor for NANOG concentration in the cells. To test this possibility, we analyzed the NANOG binding sequences in the *Fgfr2* locus. Two NANOG binding regions (NBR) with multiple NANOG binding sequences were identified in the *Fgfr2* locus from the ChIP-seq (Karwacki-Neisius et al., 2013), NBR1 at 1.4 kb, and NBR2 at -0.2 kb relative to TSS of *Fgfr2*. NBR1 and NBR2 were deleted in TNERT (Figure 4D-E, S4D-E). Autoregulation was operational in TNERTNBR1-/- albeit at reduced strength, whereas it was abolished in TNERTNBR2-/- (Figure 4F), suggesting that NBR2 is essential for the binding of NANOG and activation of *Fgfr2* to trigger autoregulation. Together, our data suggest dose-responsive induction of *Fgf4*, *Fgfbp1*, and *Fgfr2* by NANOG. The *Nanog*-high cells secrete more FGF4 and FGFBP1, also express higher FGFR2 receptors. The FGF4 in presence of FGFBP1 binds to FGFR2 to enhance FGF signaling in *Nanog*-high cells to activate pERK1/2 and repress *Nanog*. The *Nanog*-low cells express relatively low FGFR2, resulting in weak FGF signaling and the absence of autoregulation (Figure 4G). We propose that FGFR2 distinguish the *Nanog*-high cells from the low cells to activate autoregulation predominately in *Nanog*- high cells.

ERK1/2 interacts and recruits NONO to repress *Nanog* transcription.

The FGF signaling cascade leads to phosphorylation of ERK1/2. pERK could activate downstream targets like *Tcf15* to repress *Nanog* (Davies et al., 2013) or ERK can recruit chromatin regulators like NONO to induce poised pol2 state in developmental bivalent genes (Ma et al., 2016). To examine these possibilities in autoregulation, we deleted *Tcf15* and *Nono* in TNERT (Figure 5A, S5A, B). Unlike in TNERTTcf15-/- cells, OHT treatment failed to repress *Nanog*:GFP in TNERTNono-/- cell indicating essential role of NONO in autoregulation (Figure 5B, S5C). pERK1/2 was substantially reduced in TNERTNono-/- despite OHT induction, unlike in TNERT (Figure 5C, S5D). Endogenous immunoprecipitation showed an interaction between NONO and ERK1/2 in the presence or absence of NANOG (Figure 5D). NONO colocalizes with ERK1/2 to bivalent developmental genes to maintain poised POL2 (Ma et al., 2016). Although *Nanog* is an actively transcribed gene lacking bivalent marks, the indispensability of NONO and pERK1/2 for autoregulation prompted us to investigate if they bind to *Nanog* and repress its transcription. The ChIP-seq data analysis (Ma et al., 2016; Tee et al., 2014) indicated NONO and ERK1/2 binding on the *Nanog* (S5E). We induced or repressed the pERK1/2 by treatment of E14Tg2a cells with FGF4 or PD respectively (Figure 5E) and analyzed the occupancy of NONO, pERK1/2, POL2, H3K4me3, and H3K27me3. The Transcription Start Site (TSS) and 5 kb upstream region (-5kb) are the two hubs of transcription factor binding and control of *Nanog* transcription (Chen et al., 2008; Loh et al., 2006). We performed ChiP-qPCR analysis with multiple primer sets spanning the -5.8 kb to +1.5 kb region relative to TSS (Figure 5F). pERK1/2 binding was detected in immediate downstream regions of the -5kb, and TSS. pERK1/2 binding was reduced significantly in PD and enhanced in FGF4 suggesting pERK1/2 binding to *Nanog* is dependent on FGF activity (Figure 5G). NONO binds to *Nanog* at the TSS and its downstream, which is enhanced in FGF4 and abolished in PD treatment suggesting pERK1/2 recruits NONO to *Nanog* (Figure 5H). POL2 occupancy seen in TSS and downstream region was reduced in FGF4 and enhanced in PD treatment. This suggested active transcription of *Nanog* in PD and repression in FGF4 (Figure 5I). This was further corroborated with enhanced enrichment of the transcription activating histone mark H3K4me3 in PD (Figure 5J) and enrichment of transcription repressive mark H3K27me3 at the -5kb region of the *Nanog* in FGF4 treatment (Figure 5K). pERK1/2 phosphorylates

NANOG, USP21 and affects NANOG stability and transactivation capability (Brumbaugh et al., 2014; Jin et al., 2016; Kim et al., 2014). In agreement with NANOG destabilization by pERK1/2 (Brumbaugh et al., 2014; Kim et al., 2014; Pokrass et al., 2020), The half-life of NANOG was significantly compromised in FGF4 treated cells but enhanced in PD (Figure 5L, S5F), suggesting that the FGF/ERK represses *Nanog* transcription and also affects NANOG stability. Collectively, these data suggest that FGF signaling activates pERK1/2 and its binding onto *Nanog* in a concentration-dependent manner. The recruitment of NONO to *Nanog* is dependent on the pERK1/2, NONO recruitment to *Nanog* is negligible in absence of pERK1/2. In the presence of pERK1/2-NONO, the POL2 loading on *Nanog* and its transcription activity is reduced resulting in repression of *Nanog* transcription. In the absence of active FGF signaling, pERK1/2-NONO occupancy on the *Nanog* is decreased permitting increased POL2 loading and transcription activation of the *Nanog*. The destabilization of NANOG by pERK1/2 further diminishes its ability to activate its promoter (Figure 5M).

FGF autocrine signaling regulates heterogeneity and monoallelic expression of Nanog.

The ESCs cultured in Serum+LIF on gelatin exhibit *Nanog* heterogeneity (Chambers et al., 2007; Filipczyk et al., 2013) which is lost when cultured on feeders or 2i (Faddah et al., 2013; Marks et al., 2012; Miyanari and Torres-Padilla, 2012). FGF signaling is substantially but discontinuously inhibited in 2i, leading to near homogeneity of *Nanog*. The loss of heterogeneity on feeders could be due to the induction of *Nanog* expression by the extracellular matrix (ECM)-integrin signaling (Lee et al., 2010). Alternately FGF4 might be titrated out by the FGFRs on the feeders or by ECM secreted by the feeders rendering it unavailable for inducing autoregulation resulting in loss of heterogeneity. To evaluate these possibilities, we cultured TNGA in presence of FGF4 and PD on gelatin or feeders. The *Nanog*:GFP was heterogeneous in SL on gelatin and nearly homogenous on feeders; it was homogenous in SLPD and 2i on gelatin and feeders. it was repressed further in presence of FGF4 vis-à-vis SL on gelatin. The *Nanog*:GFP was heterogeneous even in cells cultured on feeders in presence of FGF4, suggesting that heterogeneity could be induced even on feeders in presence of an excess of FGF4 (Figure 6A). This discounts any major role for ECM-integrin mediated activation of *Nanog* expression contributing to the loss of heterogeneity on feeders. To negate possibilities of variations due to targeting strategies in the reporter cell lines (Faddah et al., 2013), we analyzed *Nanog* heterogeneity in E14Tg2a cells. Consistent with

the observations in TNGA, the NANOG expression was homogenous in cells cultured in SLPD, 2i, and SLSU5402 on gelatin or feeders, and in SL on feeders (Figure S6A). The NANOG expression was heterogeneous in SL on gelatin and FGF4 was sufficient to induce heterogeneous NANOG expression in cells cultured on feeders (Figure 6B). Other growth factors like Insulin, EGF, and bFGF which can activate MEK1/2 also induced varying degrees of *Nanog* heterogeneity on feeders (S6A). *Nanog* expression was homogeneous in cells lacking FGF4 and FGFR2. Recombinant FGF4 substitution in media was sufficient to repress the *Nanog* and induce heterogeneity in FGF4-/- cells (Figure 6C). To quantify these observations, we generated OGNM cell line, where a randomly integrated *Oct4*-GFP transgene expression marks undifferentiated ES cells. The *Nanog* expression is reported by a T2AmCherry integrated in-frame with the last amino acid coding sequence of a *Nanog* allele (Figure 6D, S6B). The OGNM was cultured on gelatin or feeder or Feeder Secreted Matrix (FSM) and analyzed by FACS, to study the role of these substrates in *Nanog* heterogeneity. GFP expressing ES cells were gated and analyzed to avoid the feeders. Around 50% of cells cultured on gelatin expressed T2AmCherry, which increased to 64% on feeders and 55% on FSM. Since the feeder contains feeder cells and FSM, T2AmCherry expression was increased by 9% over the FSM (Figure 6E, S6D), suggesting that the diminished heterogeneity observed on the feeder is an additive impact of the FSM and feeder cells. FGF4 repressed *Nanog* and enhanced heterogeneity on feeders and FSM. The Nanog expression was homogenous in 2i and PD on all substrates. Repression of *Nanog* in FGFR inhibitor SU5402 was significantly lower than PD (Figure 6E, S6D). EGF, bFGF, and Insulin repressed *Nanog* expression (S6C-D) suggesting MEK1/2 may be predominately activated by FGF signaling, but other growth factors can also contribute to the MEK1/2 activity in ESCs. We propose that the feeder cells and the matrix secreted by the feeders titrate out the FGF4 secreted by the ES cells and interrupt autoregulation of *Nanog* resulting in loss of heterogeneity of *Nanog*.

Monoallelic expression of *Nanog* is suggested to be underlying mechanisms for *Nanog* heterogeneity in ES cells and the embryos (Filipczyk et al., 2013; Marks et al., 2012). To analyze the expression of both the alleles of *Nanog*, we integrated an iRFP coding sequence in one allele and a GFP coding sequence in another allele in-frame with the last coding sequence of the *Nanog* to generate NANOGiRFP and NANOGsfGFP fusion protein from the two alleles (NsGiR) (Figure 6F, S6E). Around 32% of the cells exhibited biallelic expression or no expression (32%) and the rest showed monoallelic expression (36%) in SL. CHIR reduced the monoallelic population (25%) and enhanced both the biallelic and non-expressing populations. The reduced MEK1/2 activity in 2i and PD leads to biallelic expression in 90%

of the cells. Around 75% of the cells show biallelic expression in SU5402 treatment, with a significant population either showing monoallelic or no expression of *Nanog*. This further strengthens the suggestion that other growth factor signaling pathways may be feeding to MEK1/2 activity in ESCs. FGF4 significantly repressed both biallelic as well as monoallelic expression of *Nanog* leading to loss of *Nanog* expression in 50% of the cells (Figure 6G). Together our data suggest that the FGF autocrine-driven *Nanog* autoregulation is interrupted by the FSM on feeders or by MEK1/2 inhibitor in 2i leading to loss of *Nanog* heterogeneity and monoallelic expression. This also establishes the primary role of feeder cells and FSM in the regulation of *Nanog* expression.

DISCUSSION

The inhibition of MEK1/2 and GSK3β in the ground state (2i) attenuates *Nanog* heterogeneity and monoallelic expression (Filipczyk et al., 2013; Nichols et al., 2009; Wray et al., 2010). Surprisingly, autorepression remains functional in 2i, discounting the role of MEK1/2 and GSK3β in *Nanog* autorepression (Navarro et al., 2012). We attribute the highest possible de-repression of *Nanog* locus to a consistent low MEK1/2 activity in SLPD, unlike in 2i. Wnt signaling can activate MEK1/2 at multiple levels (Yun et al., 2005), hence activation of MEK1/2 in presence of CHIR may be mediated by downstream components of Wnt signaling. We suggest that the inhibition of MEK1/2 prevents differentiation in 2i, but a time-dependent increase in MEK1/2 activity is significant and sufficient to facilitate *Nanog* autoregulation. Our findings open up the plausibility of other molecular processes regulated by MEK1/2 activity to be functional in 2i.

In this study, we show that FGF autocrine signaling and its components are essential for *Nanog* autoregulation. *Nanog* is vital for the secretion of FGF4 and endoderm differentiation by cell-autonomous mechanisms (Frankenberg et al., 2011; Messerschmidt and Kemler, 2010). We show, NANOG binds to the promotors of *Fgf4*, *Fgfr1*, *Fgfr2*, and *Fgfbp1*; and induce their expression. As speculated earlier, NANOG targets-ESRRB and KLF4 may also induce some of the FGF signaling components, contributing to FGF signaling (Lakatos et al., 2014). Our data suggest that *Nanog* autoregulation is triggered above a threshold of NANOG, thereafter the intensity of repression is dependent on the levels of NANOG in the cells.

In a subpopulation of ES cells expressing high NANOG; NANOG activates the expression of *Fgf4*, *Fgfr2*, and *Fgfbp1*, leading to a state of high NANOG-high FGFR. The higher ERK1/2

activity induced by high FGFR in these cells leads to the destabilization of NANOG. The *Nanog* transcription is also decreased by transcriptional repression by pERK1/2-NONO, leading to a state of low/medium NANOG-high FGFR/ERK. In embryos, such cells may exit pluripotency to form primitive endoderm. In cell culture, such cells might continue to self-renew in presence of LIF. The reduced NANOG in these cells cannot anymore activate FGF signaling components leading to a low NANOG-low FGF/ERK state. The loss of FGF/ERK in such cells releases repression of *Nanog* and permits activation of *Nanog* by other transcription factors leading to cells with a high NANOG-low FGF/ERK state. This cycle of activation of FGF signaling by NANOG and repression of *Nanog* by FGF signaling might lead to heterogeneity of *Nanog* and heterogeneity of FGF/ERK (Figure 7A). ERK signaling heterogeneity is suggested to be a vital determinant of fate choice in ICM and ES cells (Bessonnard et al., 2014; Kang et al., 2017; Molotkov et al., 2017; Pokrass et al., 2020; Simon et al., 2020). The ERK heterogeneity has been suggested to originate due to differential local concentrations of FGF4 or heterogeneous expression of receptors FGFRs (FGFR1, FGFR2) or by negative feedback regulators (ETV5, DUSP1/6). Since FGFR1 is relatively uniformly expressed in the epiblast (Kang et al., 2017; Molotkov et al., 2017) and ESCs. Our findings may provide the basis of heterogeneous expression of FGFR2 and FGF4 in ESCs, which is dependent on NANOG concentration. The carrier protein FGFBP1 may locally enhance FGF signaling to induce ERK heterogeneity similar to heparan sulfate proteoglycans (Galanternik et al., 2015). We propose that reciprocal regulation of *Nanog* by FGF signaling and FGF signaling by NANOG as the basis for both NANOG and ERK heterogeneity.

Contradicting reports on *Nanog* heterogeneity (Chambers et al., 2007; Faddah et al., 2013; Filipczyk et al., 2013; Smith, 2013) attribute it to genetic manipulation strategies or culture on feeders or gelatin. Our study demonstrates that *Nanog* heterogeneity is induced by *Nanog* autoregulation triggered FGF autocrine signaling. The feeder cells and feeder secreted matrix interrupt this autoregulation to abolish heterogeneity (Figure 7B). *Nanog* autoregulation was speculated to regulate allelic switching and FGF4 signaling was considered dispensable for autorepression (Fidalgo et al., 2012; Navarro et al., 2012). Our study suggests that FGF autocrine signaling is essential for *Nanog* autoregulation and allelic switching (Figure 7C). We suggest that *Nanog* autoregulation is the molecular basis for *Nanog* heterogeneity.

Taken together, we demonstrate an essential role for FGF autocrine signaling in *Nanog* autoregulation, and different facets of *Nanog* regulation are intertwined and governed by FGF autocrine signaling.

Acknowledgments

HTK was supported by a fellowship from ICMR (India), DJ, VVV, MS was supported by a fellowship from UGC (India). RSR was supported by DBT grant No: BT/PR14064/GET/119/16/2015. PCS was supported by WT/DBT IA grant No: 500053/Z/09/Z. We thank the Microscopy, and FACS core facilities of CCMB for the support extended to carry out this work. We thank Ian chambers, D P Kasbekar, and V R Chalamcharla for constructive comments on the manuscript.

Author contributions

Conceptualization, H.T.K, and P.C.S Methodology, H.T.K and P.C.S; Investigation, H.T.K, R.S.R., V.V.V., and G.S.; Writing – Original Draft, H.T.K. and P.C.S.; Writing – Review & Editing, H.T.K., and P.C.S.; Funding Acquisition, P.C.S.; Resources, H.T.K, R.S.R., M.S., and D.J.; Visualization, H.T.K, and D.J.; Supervision, P.C.S.

Declaration of interest:

The authors declare no competing interests.

Figure titles and legends:

Figure 1: Residual MEK1/2 activity in ground state prevents complete derepression of *Nanog*. (A) (left) FACS profiles of TNGA cultured in indicated conditions for 3 passages. The cells were cultured in Serum+LIF (SL) in presence of the 1 μM MEK1/2 inhibitor - PD0325901 (SLPD) or 3 μM GSK3β inhibitor -CHIR99021 (SLCHIR) or in serum-free media - N2B27 with PD0325901, CHIR99021, and LIF (2i). (right) *Nanog*:GFP population median of TNGA (n=4). (B) (left) FACS profiles of Tβc44Cre6 cultured in indicated conditions for 3 passages. TβC44Cre6 is a *Nanog* null cell line, where β–*geo* cassette is inserted into one allele and GFP into another allele of the *Nanog* gene. (right) *Nanog*:GFP population median of Tβc44Cre6 (n=3). (C) FACS profile of NANOG-iRFP protein in

NiRFP2A cells cultured in indicated conditions for 3 passages. (D) RT-qPCR of pluripotency factors in indicated conditions (SL2i= SL+ PD0325901+CHIR99021). (E) RT-qPCR analysis of pre- mRNA of *Nanog* and *Oct4*. (F) (left)Western blot of NANOG, OCT4, and SOX2. (right) Relative NANOG levels as estimated by densitometry (n=8). (G) Western blot of pERK1/2 and ERK1/2 at 0, 1, 4, 8, 12, 16, and 24 hrs after media change in indicated treatments. (H) Western blot of pERK1/2 and ERK1/2 in SLPD, SLCHIR, 2i, and SL2i after 8, 12, 16, and 24 hrs of culture relative to SL, where the cells in SL were harvested 24 hrs after the media change. (I) (left)Western blot of pERK1/2 and ERK1/2 in 1μM PD and increasing concentrations of CHIR in serum-free N2B27 media. (right) Relative pERK1/2 levels (n=3). (J) (left)Western blot of pERK1/2 and ERK1/2 in 3μM CHIR and increasing concentrations of PD in serum-free N2B27 media. (right) Relative pERK1/2 levels (n=6). All error bars in the figure represent s.e.m. See also Figure S1.

Figure 2: FGF autocrine signaling pathway components are essential for *Nanog* autoregulation. (A) (left) Schematic depiction of Tamoxifen (OHT) inducible TNERT cell line. (Middle) FACS profile of TNERT treated with OHT (red) or no OHT (blue). (Right) *Nanog*:GFP population median of TNERT (n=3). (B) (left) Schematic of NsGFPDiN cells reporting NANOG-GFP fusion protein and carrying a Doxycycline- inducible FaNANOG transgene. (Middle) FACS profiles of NsGFPDiN after 48 hrs with Doxycycline (red) or no Doxycycline (blue) treatment. (Right) *Nanog*:GFP population median of NsGFPDiN (n=3). (C) FACS profiles of TNERT, NsGFPDiN, and TDiN treated with 2μM SU5402, with OHT/Doxycycline (red) or no OHT/Doxycycline (blue). (D) Heat map representing transcript levels (FPKM) of *Fgfbp1* from 8-cell to blastocyst stage analyzed from the single-cell sequencing data. (E) Schematic depiction of TNERTFgfr1-/-, TNERTFgfr2-/, TNERTFgf4-/-, and TNERTFgfbp1-/- cell lines, which are derivatives of TNERT where *Fgfr1, Fgfr2, Fgf4,* and *Fgfbp1* are knocked out respectively. (F) FACS profiles of TNERT, TNERTFgfr1-/-, TNERTFgfr2-/-, TNERTFgf4-/-, and TNERTFgfbp1-/- cells, treated with OHT (red) or no OHT (blue). All error bars in the figure represent s.e.m. See also Figure S2.

Figure 3: *Nanog* enhances expression of FGF autocrine signaling pathway components. (A) RT-qPCR showing relative transcript levels after 0, 0.5, 1, 2, 4, 8, 12 and 18 hrs OHT treatment in TNERT (n=3). (B) RT-qPCR of relative levels of pre- mRNA at the above indicated time points after OHT treatment in TNERT (n=3). (C) ChIP analysis of NANOG on

Fgf4, *Fgfbp1*, *Fgfr1*, *Fgfr2*, and *Nanog* genes in E14Tg2a cells cultured in SL or SLPD for 48 hrs (n=4). (D) ChIP analysis of NANOG on promotors of above- indicated loci in EDiN cells cultured in Doxycycline (red) or no Doxycycline (blue) for 48 hrs (n=3). (E) Western blot of FGFR1, FGFR2, and pERK1/2 in TNERT after 18 hrs treatment with (red) or no OHT (blue) (n=3). (F) FACS analysis of FGFR2 on the cell surface of TNERT treated with (red) or no OHT (blue) (n=3). (G-H) ELISA-based relative quantification of FGF4 (G) and FGFBP1 (H) in conditioned media from TNERT treated with or no OHT (n=3). (I) Schematic of conditioned media experiment. (J) FACS analysis of Tβc44Cre6 cell line in conditioned media collected from TNERT treated with OHT after 0, 18, 24, and 48 hrs (K) (left) FACS analysis of TNERTZfp281-/- cells treated with (red) or with no OHT (blue) treatment. (right) *Nanog*:GFP population median of TNERTZfp281-/- (n=3). (L) FACS analysis of Tβc44Cre6 cell line in conditioned media from, TNERT+OHT 0 hrs, TNERTFGF4-/-, Tβc44Cre6 48 hrs, E14Tg2a- FGF4-OE (overexpression) 48 hrs, TNERT+OHT 48 hrs and 50ng/ml FGF4. All error bars in the figure represent s.e.m. See also Figure S3.

Figure 4: NANOG-induced FGFR2 triggers autoregulation predominately in the ES cell population with higher *Nanog* expression. (A) (top) FACS profile of TNERT, the position of the gates indicates the 10% low-*Nanog*:GFP (LN) and 10% high-*Nanog*:GFP (HN) population sorted for culture. (bottom left) FACS profiles of LN and HN after 18 hrs culture in SL. LN (dark green), HN (dark maroon) in SL, and LN (light green), HN (light maroon) in SL+ OHT. (bottom right) *Nanog*:GFP population median of TNERT (n=3). (B) FACS profile of E14Tg2a cultured in SL or SLPD for 48 hrs and co- immunostained with anti-NANOG and anti-FGFR1 or anti-FGFR2 antibodies. r-values represent the average of 3 independent experiments (n=3). (C) (left) FACS profile of E14Tg2a immunostained with anti-NANOG and anti-FGFR2 antibody, the gates mark the 10% low-NANOG (LN) and 10% high-NANOG (HN) population. (right) Histogram depicting the FGFR2 expression profiles in the gated LN and HN cell population (n=3). (D-E) Schematic representation of TNERTNBR1-/- (D) and TNERTNBR2-/- (E) cells, in which NANOG binding sequences at +1.4 kb (NBR1) and -0.2 kb (NBR2) are deleted respectively. (F) (Top) FACS profiles of TNERT, TNERTNBR1-/-, and TNERTNBR2-/- with (red) or no OHT treatment (blue). (bottom) *Nanog*:GFP population median of TNERT, TNERTNBR1-/- and TNERTNBR2-/- with or no OHT treatment. (G) A cartoon depicting *Nanog* autoregulation in *Nanog*-high cells. The *Nanog*-high cells secrete more FGF4 and FGFBP1. They contain higher levels of FGFR2 on

the surface and hence more sensitive to the FGF ligand triggering a stronger FGF signaling. The increased pERK1/2 in these cells recruit NONO to the *Nanog* locus and represses *Nanog* transcription. The *Nanog*-low cells secrete very little FGF4 and FGFBP1 and present fewer FGFR2 on their surface and less sensitive to FGF signaling. The pERK1/2 levels in *Nanog*-low cells are insufficient to execute *Nanog* autoregulation. All error bars in the figure represent s.e.m. See also Figure S4.

Figure 5: ERK1/2 interacts and recruits NONO to repress *Nanog* transcription. (A) Schematic of TNERTNono-/-cell line; a derivative of TNERT in which *Nono* is knocked out. (B) FACS profile of TNERTNono-/- treated with or no OHT (n=3). (C) Western blot of pERK1/2 and ERK1/2 in TNERT and TNERTNono-/- cells treated with or no OHT (n=3). (D) Immunoprecipitation analysis showing interactions between ERK1/2 and NONO in the presence or absence of *Nanog* induction by Doxycycline in TDiN cells. (E) (left) Western blot of pERK1/2 and ERK1/2 in E14Tg2a cells treated with PD or FGF4. (right) Relative levels of pERK1/2 in E14Tg2a cells treated with PD or FGF4 (n=4). (F) Schematic representation of *Nanog* locus comprising the -6.0 to +2kb region. The vertical bars represent relative positions of primer pairs used for ChiP-qPCR analysis. S1-S6 are located upstream of the TSS, S7 primer pair is located around TSS, S8 and S9 are located downstream in the first intron. (G-K) ChIP-qPCR analysis of pERK1/2 (G), NONO (H), Pol2 (I), H3K4me3 (J) and H3K27me3 (K) on *Nanog* 5' region in E14Tg2a cells (blue), treated with FGF4 (green) and with PD (pink) (n=3). (L) Cycloheximide chase assay of NANOG in SL, SLPD, and SLFGF4 in E14Tg2a cells. (M) A cartoon illustrating the repression of *Nanog* by FGF signaling and derepression of *Nanog* in absence of Fgf signaling. The FGF4 activates the Fgf signaling cascade, results in phosphorylation of ERK1/2. pERK1/2 interacts and recruits NONO to *Nanog* promoter and represses transcription of *Nanog*. pERK1/2 also affects the stability of the NANOG. In absence of FGF4, the pERK1/2 levels decrease resulting in enhanced stability of NANOG and transcription of *Nanog* locus by NANOG and other pluripotency factors resulting in derepression of *Nanog* locus. All error bars represent s.e.m. See also Figure S5.

Figure 6: FGF autocrine signaling regulates *Nanog* heterogeneity and monoallelic expression. (A) *Nanog*:GFP fluorescence in TNGA cultured on gelatin or feeders in SL, SLPD, SLFGF4, and 2i (n=3). Scale bars represent 75μM. (B) Immunofluorescence of

NANOG and OCT4 in E14Tg2a cells cultured on gelatin or feeders in SL, SLPD, and SLFGF4. Areas are marked to highlight the loss of NANOG. Scale bars represent 75μM. (C) Immunofluorescence of NANOG and OCT4 in E14Tg2a, *Fgfr2*-/- ESCs, *Fgf4*-/- ESCs, and *Fgf4*-/- ESCs rescued with Ef1α–*Fgf4* transgene. The marked area highlights the loss of NANOG. Scale bars represent 75μM. (D) Schematic of OGNM cell line with *Oct4*-GFP transgenic reporter and T2A-mCherry reporting one of the *Nanog* alleles. (E) FACS profiles of OGNM cultured in SL, SLFGF4, SLSU5402, 2i, and SLPD on gelatin (top), on feeders (middle), and FSM (bottom). (F) Schematic of NsGiR cell line, with allele-specific NANOG protein reporters. One allele of *Nanog* reports as NANOGiRFP fusion protein and the other as NANOGsfGFP fusion protein. (G) FACS profiles of NsGiR cell line cultured in SL, SLCHIR, 2i, SLSU5402, SLFGF4, and SLPD. See also Figure S6.

Figure 7: A cartoon illustrating the role of FGF autocrine signaling in *Nanog* autoregulation, heterogeneity, and monoallelic expression. (a) A subpopulation of ES cells with high-*Nanog* induce expression of FGF signaling components- *Fgf4*, *Fgfbp1*, and *Fgfr2*. FGF4 and FGFBP1 are secreted out of the cells. The FGFR2 is retained on the cells leading to a high NANOG-high FGFR state. Higher FGFR activates FGF signaling in these cells resulting in enhanced pERK1/2. The pERK1/2 leads to destabilization of NANOG and recruits NONO to *Nanog* locus to repress its transcription resulting in a low/medium NANOG-high FGF/pERK state. The repression of *Nanog* and reduced NANOG levels diminishes activation of FGF signaling components, leading to a low NANOG-low FGFR state, with low pERK1/2. The diminished pERK1/2 releases the repression on the *Nanog* and enables stabilization of NANOG. This permits transcriptional activation of *Nanog* locus by pluripotency factors, increasing the expression of *Nanog* resulting in a low/medium NANOG-low FGF/pERK state. Unrestricted induction of *Nanog* in low pERK1/2 state results in enhanced activation of *Nanog* resulting in a high-*Nanog* expressing cells. (b) A cartoon showing heterogeneous expression of *Nanog* in ESCs cultured on gelatin. FGF4 and FGFBP1 are free to activate FGF autocrine/paracrine signaling to induce *Nanog* autoregulation resulting in *Nanog* heterogeneity. In feeders or FSM, FGF4 is either titrated out by FGFRs on feeder cells and extracellular matrix rendering it unavailable for triggering FGF autocrine signaling to induce *Nanog* autoregulation. In the absence of *Nanog* autoregulation, most of the cells continuously express *Nanog* resulting in loss of heterogeneity. (c) Low FGF autocrine signaling prevents pERK1/2 and repression of *Nanog* locus resulting in biallelic expression. An increase in FGF

autocrine signaling activates ERK1/2 and leads to monoallelic expression. A further increase in FGF signaling results in complete repression of the *Nanog* locus.

Methods:

Cell Culture

The cell lines used in this study are listed in the resource table and their origin is depicted in supplemental flowchart 1. All the cells used in this study are derivatives of E14Tg2a ES cells (ATCC CRL1821). The cells were cultured as described earlier (Festuccia et al., 2012). 4-Hydroxytamoxifen (4-OHT) (Cat# H7904), Doxycycline (Cat# D9891), and Cycloheximide (Cat# 239764) were used at a concentration of 1 μg/ml, 1 μg/ml, and 100 μg/ml respectively. The TNERT and its derivative cell lines were treated with 4-OHT for 18 hrs except when indicated. TDiN, NsGFPDiN, and EDiN were treated with Doxycycline for 48 hrs unless indicated. CHIR99021 (CHIR) (Cat# SML1046), PD0325901 (PD) (Cat# PZ0162), and SU5402 (Cat# SML0443) were used at 3 μM, 1 μM, and 2 μM, respectively, except when indicated. FGF4 (Cat# 7460-F4-025), FGFBP1 (Cat# 1593-FB-025), Insulin (Cat# RP-10908), EGF (Cat# 01-107) and bFGF (Cat# RP-8628) were used at 50ng/ml, 50ng/ml, 100ng/ml, 25ng/ml and 10ng/ml concentrations respectively. The cells were cultured in Serum+ LIF (SL), SL+ PD (SLPD), SL+CHIR (SLCHIR), SL+SU5402 (SLSU5402), SL + PD +CHIR (SL2i) and N2B27+LIF+PD+CHIR (2i) for at least 2 passages before treating with either 4-OHT or Doxycycline.

The cells were cultured on cell culture dishes coated with 0.1% gelatin for all experiments. In experiments involving ESCs cultured on feeders, the feeder cells were seeded onto the culture dishes at least 48 hrs before seeding ESCs. To prepare feeder secrete matrix (FSM), feeder cells were seeded onto a culture dish and cultured for 4-5 days. The cells were lysed with 0.01% SDS for 30 mins followed by two washes with PBS for 30 mins each. Finally, the FSM was equilibrated with media for 30 mins. The conditioned media from the cells was collected after the specific treatments or indicated time points. The conditioned media was passed through a 0.22 μM filter and added to T*β*c44Cre6 or TNERT cells. The cells were cultured in the conditioned media for 24 hrs before FACS analysis.

Generation of Knock-out cell lines using paired CRISPR constructs: pU6-iRFP (pU6-

Cas9-T2A-iRFP-2A-PuroR) construct was engineered by replacing mCherry coding sequence with iRFP670-2A-PuroR cassette in pU6-(BbsI)-CBh-Cas9-T2A-mCherry plasmid (Addgene 64324) by Gibson assembly. For generating knock-out of a gene, two sgRNAs were designed with the expected cutting sites at least 30 bps apart to achieve deletion of at least 30 bps or more. For genotyping of the deletions, a set of genotyping primers was designed outside the deletion region flanking the sgRNA pair. The sgRNAs were designed using the UCSC genome browser and Deskgen or Benchling. The sequences of the sgRNAs and the genotyping primers are detailed in Supplemental data table 1. All sgRNAs were cloned into pU6-Cas9-T2A-iRFP-2A- PuroR plasmids. To generate a paired sgRNA construct, the U6-SgRNA cassette from one plasmid containing the sgRNA was amplified and Gibson assembled into the XbaI site of the plasmid containing the other sgRNA pair of the pair. Around 1 µg of paired sgRNA CRISPR plasmid was nucleofected in 1 million cells. The transfected cells were sorted by FACS for iRFP expression and cultured to obtain clones. The clones were genotyped by PCR using respective primer sets to identify the heterozygous and homozygous clones. The sequence of the derivation of cell lines is described in supplemental Figure 7.

Generation of Knock-in cell lines: A sgRNA encompassing the stop codon of *Nanog* was cloned into pU6-iRFP and co-transfected with the targeting vectors. Nanog-2A- mCherry targeting vector (Addgene 59995) was used for generating the OGNM cell line. The 2A-mCherry cassette was replaced with sfGFP or iRFP sequences by Gibson assembly to generate Nanog sfGFP fusion or Nanog iRFP670 fusion targeting vector respectively. Around 3 µg plasmid (targeting vector and CRISPR plasmid) were nucleofected in 3 million E14Tg2a cells. The cells were selected against G418. The derivation of cell lines is described in Supplemental Figure 7.

Real-time PCR analysis:

The RNA was extracted with TRIZOL reagent and quantified using Nanodrop2000 spectrophotometer (Thermo Fisher Scientific). One microgram of total RNA was reversed transcribed into cDNA by using superscript III. All real-time PCR was carried out with Power SYBR Green PCR master mix on the ABI prism 7900 HT sequence detection system (ABI) as per the manufacturer’s instructions. GAPDH was used as an internal control or normalizer. The data was analyzed by SDS 2.2 software provided with the instrument. The

primers used for real-time PCR are given in the supplemental data table 1.

Western blot analysis: The cells were harvested by using RIPA buffer with 25mM Tris HCl (pH 8.0), 150mM NaCl, 1%NP-40, 0.5% Sodium deoxycholate, 0.1% SDS and Complete Protease Inhibitor Cocktail Tablets (Cat# 11873580001). The protein samples were resolved by 4-20% gradient SDS-PAGE and electroblotted on to polyvinylidene difluoride (PVDF) membrane. The blot was blocked with 3% Blotto (Cat# SC-2324) for an hour and incubated overnight with a primary antibody at 4°C. Blots were washed thrice with TBST and hybridized with secondary antibody and the blots were visualized using enhanced chemiluminescence (ECL)detection kit. Western blot quantifications were performed using Image lab (Bio-rad).

Chromatin Immunoprecipitation (ChIP):

Cells were fixed by adding 270 µL of 37% formaldehyde into 10 ml of media and incubated for 10 minutes at 37^{0}C to crosslink the chromatin. Cells were washed twice with cold PBS containing protease inhibitors. Cells were scraped and harvested by centrifugation. The cell pellet was dissolved in 200 µL of SDS Lysis Buffer (1% SDS, 10 mM EDTA, and 50 mM Tris, pH 8.0) containing protease inhibitors (per 10^{6} cells) and incubated on ice for 10 min. The 25 cycles of sonication were used to shear DNA between 200 to1000 base pairs. The sample was centrifuged at 13,000 rpm for 10 min (at 4°C). The supernatant was diluted by adding 1800 µl ChIP Dilution Buffer (1.1% Triton X- 100, 1.2 mM EDTA, 16.7 mM Tris-HCl, pH 8.0, 167 mM NaCl with protease inhibitors). The 1% input was aliquoted from the supernatant. To reduce nonspecific background, diluted cell supernatant was preabsorbed for one hour at 4°C with protein A/G magnetic beads (Cat# 88803). The supernatant fraction was incubated overnight at 4°C with appropriate antibody and protein A/G magnetic beads were blocked with 4% BSA, 2µg salmon sperm DNA. The next day, pre-blocked beads were mixed with the sample and incubated for 1 hour to capture the antibodies. The supernatant was discarded and washed in the given order with 1 mL of each of the buffers - Low Salt Wash Buffer (0.1% SDS, 1% Triton X-100, 2 mM EDTA, 20 mM Tris-HCl, pH 8.0, 150 mM NaCl), High Salt Wash Buffer (0.1% SDS, 1% Triton X-100, 2 mM EDTA, 20 mM Tris-HCl, pH 8.0, 500 mM NaCl), LiCl Wash Buffer (0.25 M LiCl, 1% IGEPAL-CA630, 1% deoxycholic acid, 1 mM EDTA, 10 mM Tris, pH 8.0.), and TE buffer. DNA was eluted with elution buffer (1%SDS, 0.1M NaHCO3). The sample input and the ChIP chromatin were

reverse crosslinked with 20 µL of 5 M NaCl by heating at 65°C for 4 hours. Followed by one hour at 45°C with 10 µL of 0.5 M EDTA, 20 µL 1 M Tris- HCl, pH 6.5, and 2 µL of 10 mg/mL Proteinase K. Finally, DNA was eluted in 50 µL water using a minEleute PCR purification kit (Cat# 28006). Then 1µL of sample and input was used for qPCR analysis. The primers used for qPCR analysis were listed in supplemental data table 1.

Co-Immunoprecipitation in ES cells: 10-12 million ES cells were harvested by trypsinization, washed twice with cold PBS, and resuspended in 800 µl of CoIP Lysis Buffer (50 mM Tris-HCl, pH 67.5; 350 mM NaCl, 0.7% NP40, EDTA 0.1mM, 20% (v/v) glycerol, and protease inhibitor cocktail). The cell lysate was mixed with protein A/G magnetic beads (Cat# 88803) for 1 hour at 4°C for pre-clearing the background. Then 5% input was aliquoted and the remaining supernatant was incubated overnight with appropriate primary antibody. The protein A/G magnetic beads were blocked overnight at 4°C with 200 µl of CoIP Lysis buffer containing 4% BSA. The next day, the beads were transferred to the primary antibody incubated tubes and incubated for one hour at 4°C. The bead was washed three times with ice-cold TBS150 (50mM Tris, 150mM NaCl) and the protein was eluted with 2X sample buffer (125 mM Tris-HCl, pH 6.8**,** 4% SDS**,** 20% (v/v) glycerol, 0.004% bromophenol blue), by boiling for 5 min. The western was done for sample and input and the interaction was analyzed.

Immunocytochemistry: The cells were cultured in 24 well dishes and fixed at 70% confluency in 3.7% formaldehyde diluted in PBS for 15 mins at RT. After 3 washes with PBS, the cells were permeabilized and blocked with PBS containing 0.5% BSA and 0.3% Triton-X100 for 1 hour at room temperature. The cells were hybridized with primary antibody (1:100 dilution) in PBS containing 0.5% BSA at 4°C overnight in a humidified chamber. The cells were washed three times with PBS and hybridized to appropriate secondary antibody at 1:1000 dilution room temperature for 1hour. The nuclei were stained with DAPI in 1X PBS for 20 min at room temperature. The cells were washed thrice with PBS. The cells were layered with 100 µl of the mixture of PBS and Glycerol (1:1) and the images were acquired on the ZEISS Axio observer microscope and analyzed using ImageJ software.

ELISA Assay:

The condition media from the cell lines was collected at the respective time points. 100 µl of

the media was coated per well of 96 well of ELISA plate by incubating overnight at 4^oC. The wells were washed thrice with PBS containing 0.05% Tween-20 and blocked with PBS containing 2% BSA for one hour at room temperature. The wells were washed once with PBS and incubated with the appropriate primary antibody (1:100) for one hour. Washed thrice with PBST, appropriate HRP-labeled secondary antibody was hybridized for one hour at room temperature. The wells were washed thrice with PBST and incubated in substrate solution OPD (o-phenylenediamine dihydrochloride) (Cat# P8287) 3mg/ml with 6 µl/ml H_2O_2) for 30 min in dark. The reaction was stopped by using 2N H_2SO_4. The absorbance was measured at 492 nm in Power wave XS2 (Bio Tek instruments)

FACS analysis:

Reporter cells: Cells were trypsinized and collected by spinning at 800 rpm for 5 min. The media was removed and cells were resuspended in 300 µl of PBS containing 2% FBS at 10^6 cells/ml. The samples were analyzed in the Gallios flow cytometer (Beckman Coulter) or Fortessa flow cytometer (BD Biosciences). Sorting was performed on a MoFlo-XDP cell sorter (Beckman Coulter).

Immunostained cells: Cells were harvested by treatment with 0.5 mM EDTA and resuspended into single cells. The cells were fixed in PBS with 4% paraformaldehyde (PFA) for 20 min at room temperature. Cells were washed twice with cold PBS and incubated with methanol for 30 min for permeabilization. In the case of experiments involving analysis of FGFRs on the cell surface, the permeabilization step was excluded. Then cells were blocked with PBS containing 0.5% BSA for 60 min at room temperature. The cells were washed and hybridized to the appropriate primary antibody at 4^oC overnight. The cells were washed thrice with PBS and hybridized to the appropriate secondary antibody in PBS containing 0.5% BSA at1:1000 dilution for one hour at room temperature. The cells were washed thrice with PBS and the fluorescence profiles were acquired in the Gallios FACS analyzer (Beckman Coulter). All the FACS data were analyzed using FlowJo software (BD Biosciences).

Statistical analysis and reproducibility:

Statistical analysis was done by using a two-tailed paired or unpaired student t-test. The representation of data is in the form of means+/-SEM. The mean was calculated for more than

three independent experiments *P* value<0.05 is considered as statistically significant. * represents P<0.05, ** represents P<0.001, *** represents P<0.0001, and **** represents P<0.00001.

REFERENCES

Auciello, G., Cunningham, D.L., Tatar, T., Heath, J.K., and Rappoport, J.Z. (2013). Regulation of fibroblast growth factor receptor signalling and trafficking by Src and Eps8. Journal of cell science *126*, 613-624.

Bessonnard, S., De Mot, L., Gonze, D., Barriol, M., Dennis, C., Goldbeter, A., Dupont, G., and Chazaud, C. (2014). Gata6, Nanog and Erk signaling control cell fate in the inner cell mass through a tristable regulatory network. Development *141*, 3637-3648.

Brumbaugh, J., Russell, J.D., Yu, P., Westphall, M.S., Coon, J.J., and Thomson, J.A. (2014). NANOG is multiply phosphorylated and directly modified by ERK2 and CDK1 in vitro. Stem cell reports *2*, 18-25.

Chambers, I., Colby, D., Robertson, M., Nichols, J., Lee, S., Tweedie, S., and Smith, A. (2003). Functional expression cloning of Nanog, a pluripotency sustaining factor in embryonic stem cells. Cell *113*, 643-655.

Chambers, I., Silva, J., Colby, D., Nichols, J., Nijmeijer, B., Robertson, M., Vrana, J., Jones, K., Grotewold, L., and Smith, A. (2007). Nanog safeguards pluripotency and mediates germline development. Nature *450*, 1230-1234.

Chen, X., Xu, H., Yuan, P., Fang, F., Huss, M., Vega, V.B., Wong, E., Orlov, Y.L., Zhang, W., and Jiang, J. (2008). Integration of external signaling pathways with the core transcriptional network in embryonic stem cells. Cell *133*, 1106-1117.

Davies, O.R., Lin, C.-Y., Radzisheuskaya, A., Zhou, X., Taube, J., Blin, G., Waterhouse, A., Smith, A.J., and Lowell, S. (2013). Tcf15 primes pluripotent cells for differentiation. Cell reports *3*, 472-484.

Faddah, D.A., Wang, H., Cheng, A.W., Katz, Y., Buganim, Y., and Jaenisch, R. (2013). Single-cell analysis reveals that expression of nanog is biallelic and equally variable as that of other pluripotency factors in mouse ESCs. Cell stem cell *13*, 23-29.

Festuccia, N., Osorno, R., Halbritter, F., Karwacki-Neisius, V., Navarro, P., Colby, D., Wong, F., Yates, A., Tomlinson, S.R., and Chambers, I. (2012). Esrrb is a direct Nanog target gene that can substitute for Nanog function in pluripotent cells. Cell stem cell *11*, 477-490.

Fidalgo, M., Faiola, F., Pereira, C.-F., Ding, J., Saunders, A., Gingold, J., Schaniel, C., Lemischka, I.R., Silva, J.C., and Wang, J. (2012). Zfp281 mediates Nanog autorepression through recruitment of the NuRD complex and inhibits somatic cell reprogramming. Proceedings of the National Academy of Sciences *109*, 16202-16207.

Fidalgo, M., Shekar, P.C., Ang, Y.S., Fujiwara, Y., Orkin, S.H., and Wang, J. (2011). Zfp281 functions as a transcriptional repressor for pluripotency of mouse embryonic stem cells. Stem cells *29*, 1705-1716.

Filipczyk, A., Gkatzis, K., Fu, J., Hoppe, P.S., Lickert, H., Anastassiadis, K., and Schroeder, T. (2013). Biallelic expression of nanog protein in mouse embryonic stem cells. Cell stem cell *13*, 12-13.

Francavilla, C., Rigbolt, K.T., Emdal, K.B., Carraro, G., Vernet, E., Bekker-Jensen, D.B., Streicher, W., Wikström, M., Sundström, M., and Bellusci, S. (2013). Functional proteomics defines the molecular switch underlying FGF receptor trafficking and cellular outputs.

Molecular cell *51*, 707-722.
Frankenberg, S., Gerbe, F., Bessonnard, S., Belville, C., Pouchin, P., Bardot, O., and Chazaud, C. (2011). Primitive endoderm differentiates via a three-step mechanism involving Nanog and RTK signaling. Developmental cell *21*, 1005-1013.
Galanternik, M.V., Kramer, K.L., and Piotrowski, T. (2015). Heparan sulfate proteoglycans regulate Fgf signaling and cell polarity during collective cell migration. Cell reports *10*, 414-428.
Hamazaki, T., Kehoe, S.M., Nakano, T., and Terada, N. (2006). The Grb2/Mek pathway represses Nanog in murine embryonic stem cells. Molecular and cellular biology *26*, 7539-7549.
Hayashi, K., de Sousa Lopes, S.M.C., Tang, F., and Surani, M.A. (2008). Dynamic equilibrium and heterogeneity of mouse pluripotent stem cells with distinct functional and epigenetic states. Cell stem cell *3*, 391-401.
Jin, J., Liu, J., Chen, C., Liu, Z., Jiang, C., Chu, H., Pan, W., Wang, X., Zhang, L., and Li, B. (2016). The deubiquitinase USP21 maintains the stemness of mouse embryonic stem cells via stabilization of Nanog. Nature communications *7*, 1-15.
Kalmar, T., Lim, C., Hayward, P., Munoz-Descalzo, S., Nichols, J., Garcia-Ojalvo, J., and Arias, A.M. (2009). Regulated fluctuations in nanog expression mediate cell fate decisions in embryonic stem cells. PLoS Biol *7*, e1000149.
Kang, M., Garg, V., and Hadjantonakis, A.-K. (2017). Lineage establishment and progression within the inner cell mass of the mouse blastocyst requires FGFR1 and FGFR2. Developmental cell *41*, 496-510. e495.
Karwacki-Neisius, V., Göke, J., Osorno, R., Halbritter, F., Ng, J.H., Weiße, A.Y., Wong, F.C., Gagliardi, A., Mullin, N.P., and Festuccia, N. (2013). Reduced Oct4 expression directs a robust pluripotent state with distinct signaling activity and increased enhancer occupancy by Oct4 and Nanog. Cell stem cell *12*, 531-545.
Kim, S.-H., Kim, M.O., Cho, Y.-Y., Yao, K., Kim, D.J., Jeong, C.-H., Yu, D.H., Bae, K.B., Cho, E.J., and Jung, S.K. (2014). ERK1 phosphorylates Nanog to regulate protein stability and stem cell self-renewal. Stem cell research *13*, 1-11.
Kunath, T., Saba-El-Leil, M.K., Almousailleakh, M., Wray, J., Meloche, S., and Smith, A. (2007). FGF stimulation of the Erk1/2 signalling cascade triggers transition of pluripotent embryonic stem cells from self-renewal to lineage commitment. Development *134*, 2895-2902.
Lakatos, D., Travis, E.D., Pierson, K.E., Vivian, J.L., and Czirok, A. (2014). Autocrine FGF feedback can establish distinct states of Nanog expression in pluripotent stem cells: a computational analysis. BMC Systems Biology *8*, 1-15.
Lanner, F., and Rossant, J. (2010). The role of FGF/Erk signaling in pluripotent cells. Development *137*, 3351-3360.
Lee, S.T., Im Yun, J., Jo, Y.S., Mochizuki, M., van der Vlies, A.J., Kontos, S., Ihm, J.E., Lim, J.M., and Hubbell, J.A. (2010). Engineering integrin signaling for promoting embryonic stem cell self-renewal in a precisely defined niche. Biomaterials *31*, 1219-1226.
Loh, Y.-H., Wu, Q., Chew, J.-L., Vega, V.B., Zhang, W., Chen, X., Bourque, G., George, J., Leong, B., and Liu, J. (2006). The Oct4 and Nanog transcription network regulates pluripotency in mouse embryonic stem cells. Nature genetics *38*, 431-440.
Ma, C., Karwacki-Neisius, V., Tang, H., Li, W., Shi, Z., Hu, H., Xu, W., Wang, Z., Kong, L., and Lv, R. (2016). Nono, a bivalent domain factor, regulates Erk signaling and mouse embryonic stem cell pluripotency. Cell reports *17*, 997-1007.
Marks, H., Kalkan, T., Menafra, R., Denissov, S., Jones, K., Hofemeister, H., Nichols, J., Kranz, A., Stewart, A.F., and Smith, A. (2012). The transcriptional and epigenomic foundations of ground state pluripotency. Cell *149*, 590-604.

Messerschmidt, D.M., and Kemler, R. (2010). Nanog is required for primitive endoderm formation through a non-cell autonomous mechanism. Developmental biology *344*, 129-137.
Mitsui, K., Tokuzawa, Y., Itoh, H., Segawa, K., Murakami, M., Takahashi, K., Maruyama, M., Maeda, M., and Yamanaka, S. (2003). The homeoprotein Nanog is required for maintenance of pluripotency in mouse epiblast and ES cells. Cell *113*, 631-642.
Miyanari, Y., and Torres-Padilla, M.-E. (2012). Control of ground-state pluripotency by allelic regulation of Nanog. Nature *483*, 470-473.
Molotkov, A., Mazot, P., Brewer, J.R., Cinalli, R.M., and Soriano, P. (2017). Distinct requirements for FGFR1 and FGFR2 in primitive endoderm development and exit from pluripotency. Developmental cell *41*, 511-526. e514.
Mora-Castilla, S., Tejedo, J., Hmadcha, A., Cahuana, G.M., Martín, F., Soria, B., and Bedoya, F. (2010). Nitric oxide repression of Nanog promotes mouse embryonic stem cell differentiation. Cell Death & Differentiation *17*, 1025-1033.
Navarro, P., Festuccia, N., Colby, D., Gagliardi, A., Mullin, N.P., Zhang, W., Karwacki-Neisius, V., Osorno, R., Kelly, D., and Robertson, M. (2012). OCT4/SOX2-independent Nanog autorepression modulates heterogeneous Nanog gene expression in mouse ES cells. The EMBO journal *31*, 4547-4562.
Nichols, J., Silva, J., Roode, M., and Smith, A. (2009). Suppression of Erk signalling promotes ground state pluripotency in the mouse embryo. Development *136*, 3215-3222.
Niwa, H., Ogawa, K., Shimosato, D., and Adachi, K. (2009). A parallel circuit of LIF signalling pathways maintains pluripotency of mouse ES cells. Nature *460*, 118-122.
Ornitz, D.M., Xu, J., Colvin, J.S., McEwen, D.G., MacArthur, C.A., Coulier, F., Gao, G., and Goldfarb, M. (1996). Receptor specificity of the fibroblast growth factor family. Journal of Biological Chemistry *271*, 15292-15297.
Park, S.-J., Shirahige, K., Ohsugi, M., and Nakai, K. (2015). DBTMEE: a database of transcriptome in mouse early embryos. Nucleic acids research *43*, D771-D776.
Pereira, L., Yi, F., and Merrill, B.J. (2006). Repression of Nanog gene transcription by Tcf3 limits embryonic stem cell self-renewal. Molecular and cellular biology *26*, 7479-7491.
Pokrass, M.J., Ryan, K.A., Xin, T., Pielstick, B., Timp, W., Greco, V., and Regot, S. (2020). Cell-cycle-dependent ERK signaling dynamics direct fate specification in the mammalian preimplantation embryo. Developmental Cell *55*, 328-340. e325.
Simon, C.S., Rahman, S., Raina, D., Schröter, C., and Hadjantonakis, A.-K. (2020). Live Visualization of ERK Activity in the Mouse Blastocyst Reveals Lineage-Specific Signaling Dynamics. Developmental Cell *55*, 341-353. e345.
Smith, A. (2013). Nanog heterogeneity: tilting at windmills? Cell stem cell *13*, 6-7.
Tassi, E., Al-Attar, A., Aigner, A., Swift, M.R., McDonnell, K., Karavanov, A., and Wellstein, A. (2001). Enhancement of fibroblast growth factor (FGF) activity by an FGF-binding protein. Journal of Biological Chemistry *276*, 40247-40253.
Tee, W.-W., Shen, S.S., Oksuz, O., Narendra, V., and Reinberg, D. (2014). Erk1/2 activity promotes chromatin features and RNAPII phosphorylation at developmental promoters in mouse ESCs. Cell *156*, 678-690.
Torres-Padilla, M.-E., and Chambers, I. (2014). Transcription factor heterogeneity in pluripotent stem cells: a stochastic advantage. Development *141*, 2173-2181.
Toyooka, Y., Shimosato, D., Murakami, K., Takahashi, K., and Niwa, H. (2008). Identification and characterization of subpopulations in undifferentiated ES cell culture. Development *135*, 909-918.
van den Berg, D.L., Zhang, W., Yates, A., Engelen, E., Takacs, K., Bezstarosti, K., Demmers, J., Chambers, I., and Poot, R.A. (2008). Estrogen-related receptor beta interacts with Oct4 to positively regulate Nanog gene expression. Molecular and cellular biology *28*, 5986-5995.

Wray, J., Kalkan, T., and Smith, A.G. (2010). The ground state of pluripotency. Biochemical Society Transactions *38*, 1027-1032.
Yun, M.-S., Kim, S.-E., Jeon, S.H., Lee, J.-S., and Choi, K.-Y. (2005). Both ERK and Wnt/β-catenin pathways are involved in Wnt3a-induced proliferation. Journal of cell science *118*, 313-322.
Zhang, X., Ibrahimi, O.A., Olsen, S.K., Umemori, H., Mohammadi, M., and Ornitz, D.M. (2006). Receptor specificity of the fibroblast growth factor family: the complete mammalian FGF family. Journal of Biological Chemistry *281*, 15694-15700.

Figure 1

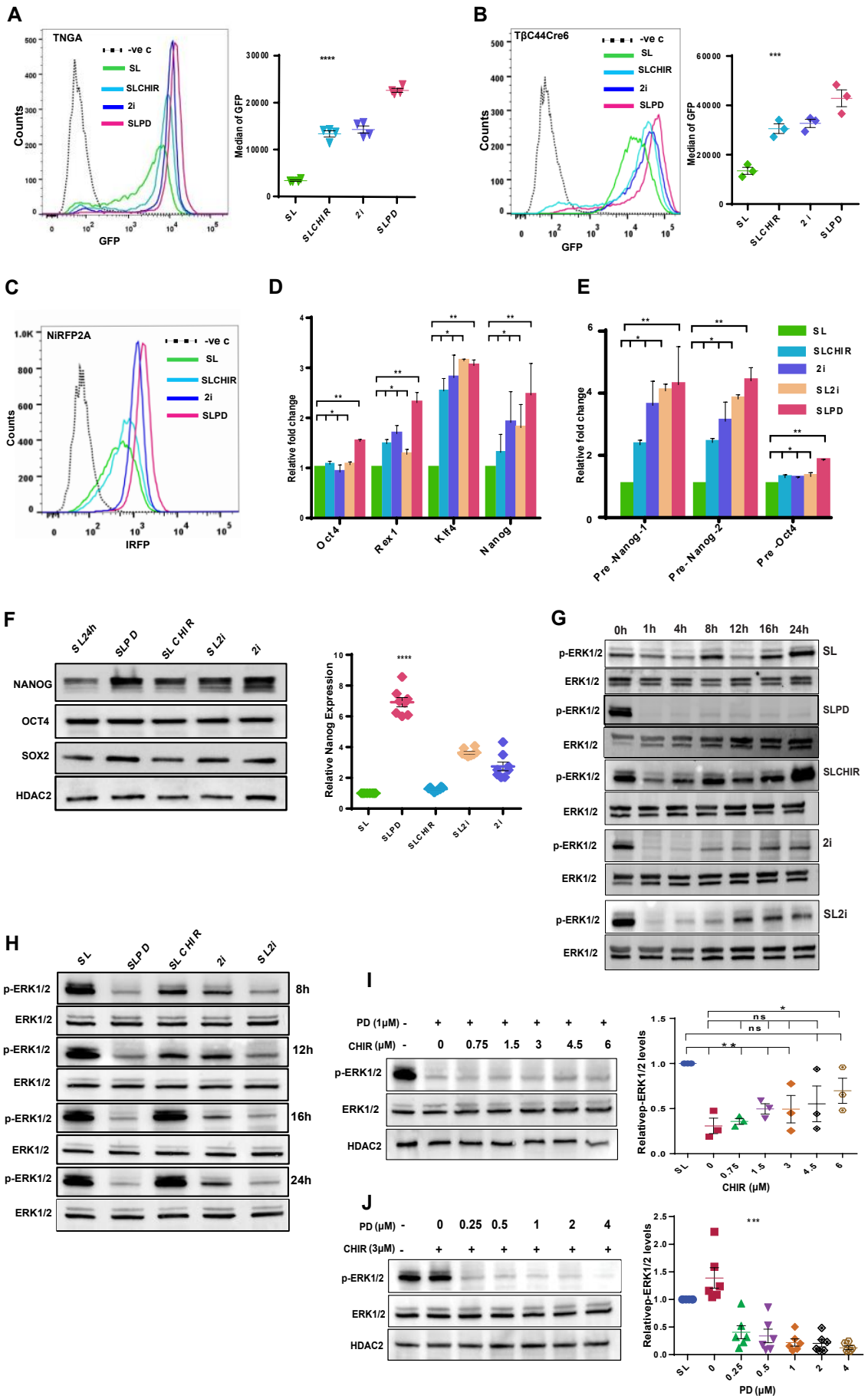
A
TNGA
-ve c
SL
SLCHIR
2i
SLPD
Counts
GFP
Median of GFP
B
TβC44Cre6
C
NiRFP2A
IRFP
D
Relative fold change
Oct4
Rex1
Klf4
Nanog
E
SL2i
Pre-Nanog-1
Pre-Nanog-2
Pre-Oct4
F
SL24h
SL CHIR
NANOG
OCT4
SOX2
HDAC2
Relative Nanog Expression
G
0h
1h
4h
8h
12h
16h
24h
p-ERK1/2
ERK1/2
H
8h
12h
16h
24h
I
PD (1μM)
CHIR (μM)
Relativep-ERK1/2 levels
J
PD (μM)
CHIR (3μM)

Figure 2

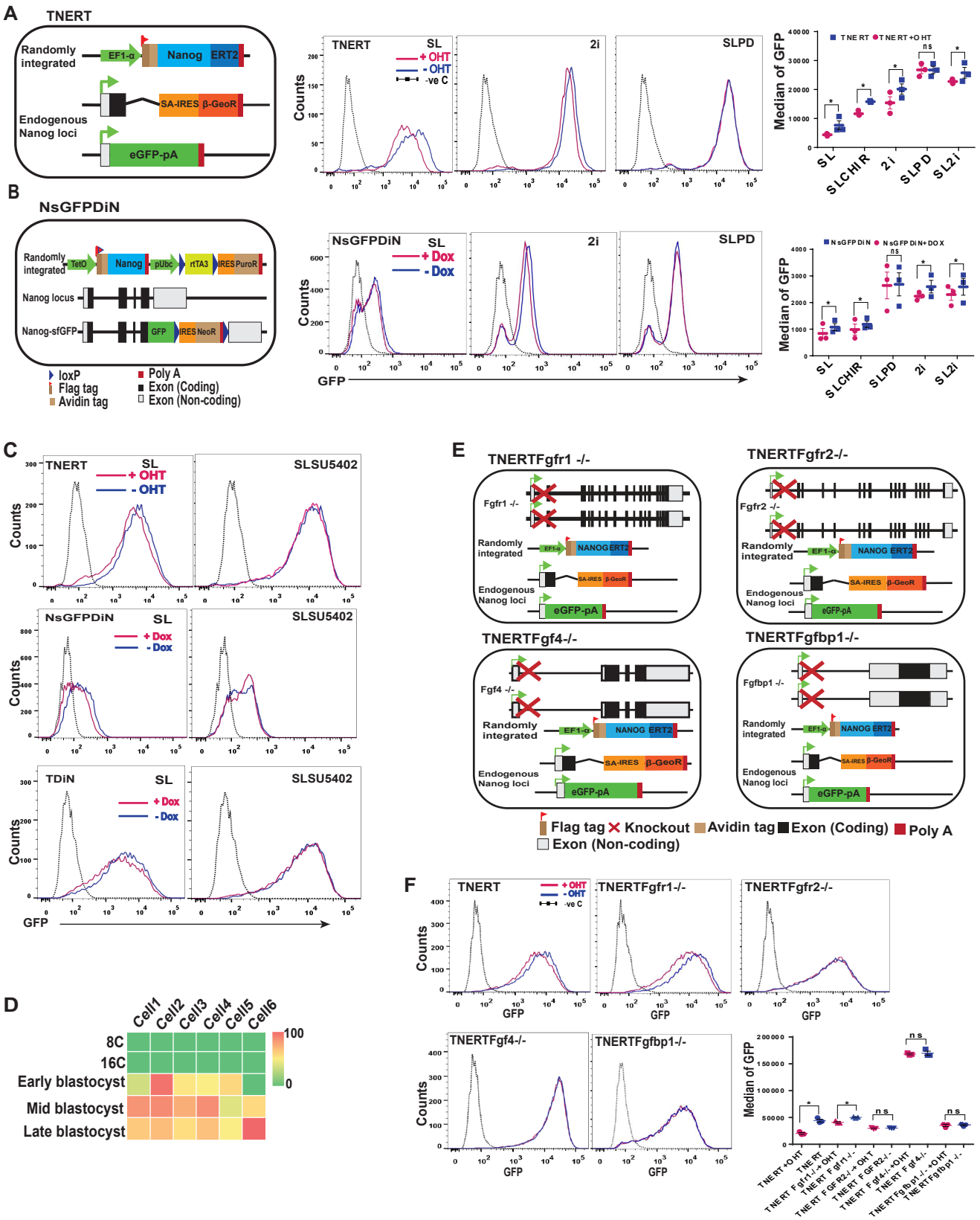
A
TNERT
Randomly integrated
EF1-α
Nanog
ERT2
Endogenous Nanog loci
SA-IRES
β-GeoR
eGFP-pA
TNERT
SL
+ OHT
- OHT
-ve C
2i
SLPD
Counts
Median of GFP
TNERT
TNERT +OHT
SL
SLCHIR
2i
SLPD
SL2i
B
NsGFPDiN
Randomly integrated
TetO
Nanog
pUbc
rtTA3
IRES PuroR
Nanog locus
Nanog-sfGFP
GFP
IRES NeoR
loxP
Flag tag
Avidin tag
Poly A
Exon (Coding)
Exon (Non-coding)
NsGFPDiN
SL
+ Dox
- Dox
2i
SLPD
GFP
NsGFPDiN
NsGFPDiN+DOX
C
TNERT
SL
+ OHT
- OHT
SLSU5402
NsGFPDiN
SL
+ Dox
- Dox
SLSU5402
TDiN
SL
+ Dox
- Dox
SLSU5402
GFP
D
Cell1
Cell2
Cell3
Cell4
Cell5
Cell6
8C
16C
Early blastocyst
Mid blastocyst
Late blastocyst
100
0
E
TNERTFgfr1 -/-
Fgfr1 -/-
Randomly integrated
NANOG
ERT2
Endogenous Nanog loci
eGFP-pA
TNERTFgfr2-/-
Fgfr2 -/-
EF1-β
TNERTFgf4-/-
Fgf4 -/-
EF1-α
TNERTFgfbp1-/-
Fgfbp1 -/-
Flag tag
Knockout
Avidin tag
Exon (Coding)
Poly A
Exon (Non-coding)
F
TNERT
+ OHT
- OHT
-ve C
TNERTFgfr1-/-
TNERTFgfr2-/-
TNERTFgf4-/-
TNERTFgfbp1-/-
Counts
GFP
Median of GFP
TNERT +OHT
TNERT
TNERT Fgfr1-/- +OHT
TNERT Fgfr1-/-
TNERT FGFR2-/- +OHT
TNERT FGFR2-/-
TNERT Fgf4-/- +OHT
TNERT Fgf4-/-
TNERT Fgfbp1-/- +OHT
TNERT Fgfbp1-/-

Figure 3

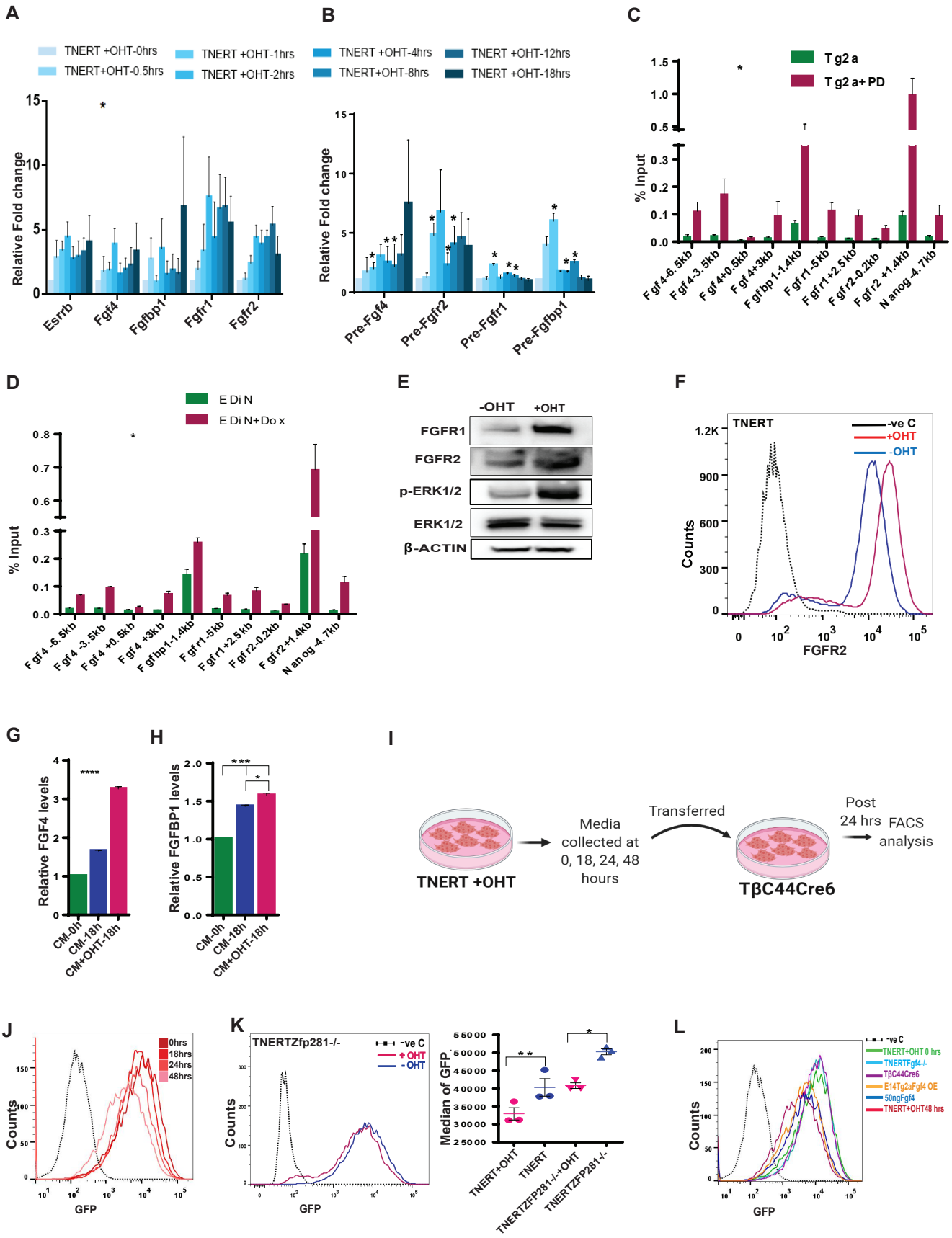
A
TNERT +OHT-0hrs
TNERT+OHT-0.5hrs
TNERT +OHT-1hrs
TNERT +OHT-2hrs
Relative Fold change
Esrrb
Fgf4
Fgfbp1
Fgfr1
Fgfr2
B
TNERT +OHT-4hrs
TNERT+OHT-8hrs
TNERT +OHT-12hrs
TNERT +OHT-18hrs
Relative Fold change
Pre-Fgf4
Pre-Fgfr2
Pre-Fgfr1
Pre-Fgfbp1
C
Tg2a
Tg2a+PD
% Input
Fgf4-6.5kb
Fgf4-3.5kb
Fgf4+0.5kb
Fgf4+3kb
Fgfbp1-1.4kb
Fgfr1-5kb
Fgfr1+2.5kb
Fgfr2-0.2kb
Fgfr2+1.4kb
Nanog-4.7kb
D
EDiN
EDiN+Dox
% Input
Fgf4-6.5kb
Fgf4-3.5kb
Fgf4+0.5kb
Fgf4+3kb
Fgfbp1-1.4kb
Fgfr1-5kb
Fgfr1+2.5kb
Fgfr2-0.2kb
Fgfr2+1.4kb
Nanog-4.7kb
E
-OHT
+OHT
FGFR1
FGFR2
p-ERK1/2
ERK1/2
β-ACTIN
F
TNERT
-ve C
+OHT
-OHT
Counts
FGFR2
G
Relative FGF4 levels
CM-0h
CM-18h
CM+OHT-18h
H
Relative FGFBP1 levels
CM-0h
CM-18h
CM+OHT-18h
I
TNERT +OHT
Media collected at 0, 18, 24, 48 hours
Transferred
TβC44Cre6
Post 24 hrs
FACS analysis
J
0hrs
18hrs
24hrs
48hrs
Counts
GFP
K
TNERTZfp281-/-
-ve C
+OHT
-OHT
Counts
GFP
Median of GFP
TNERT+OHT
TNERT
TNERTZFP281-/-+OHT
TNERTZFP281-/-
L
-ve C
TNERT+OHT 0 hrs
TNERTFgf4-/-
TβC44Cre6
E14Tg2aFgf4 OE
50ngFgf4
TNERT+OHT48 hrs
Counts
GFP

Figure 4

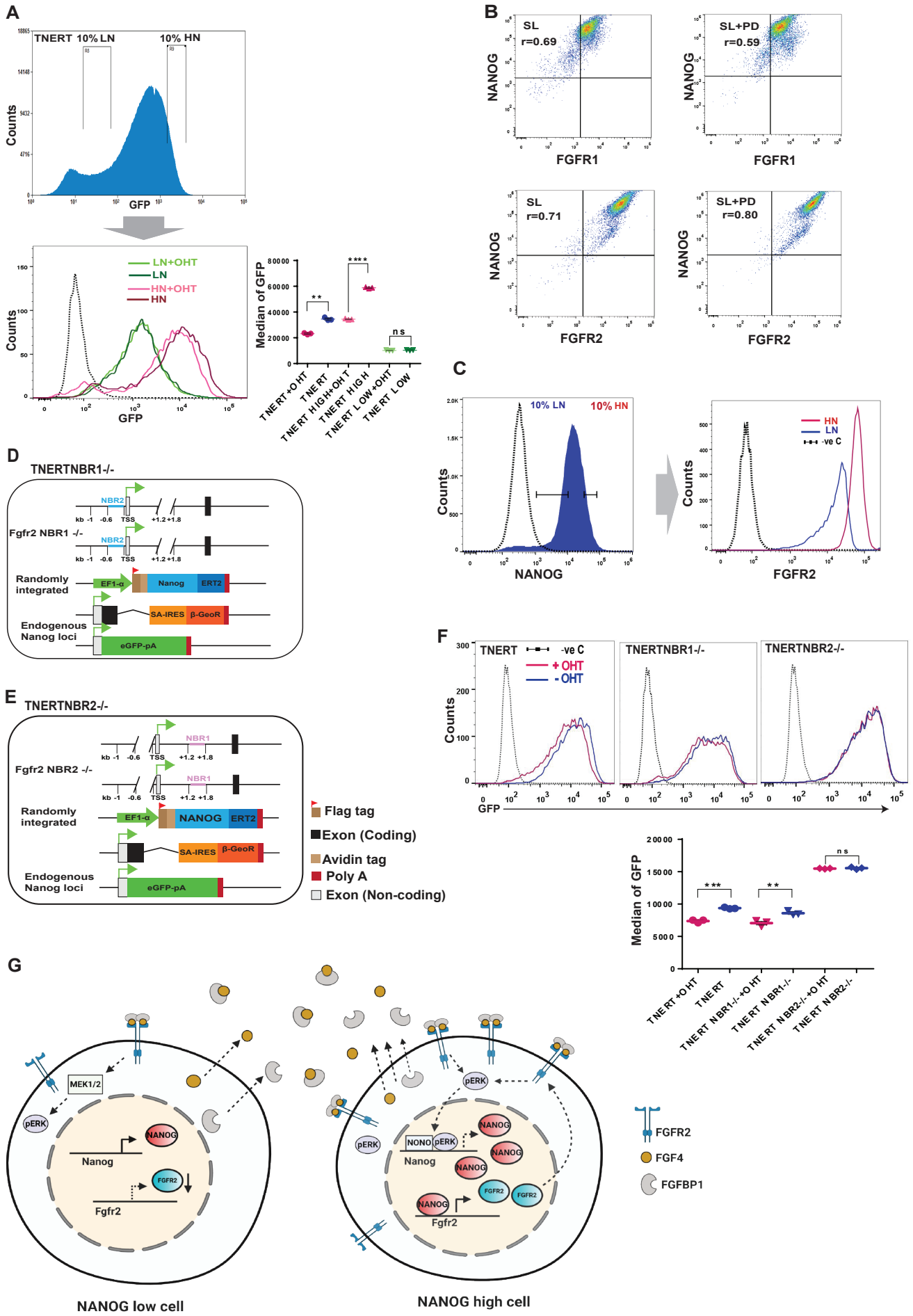
A
TNERT 10% LN
10% HN
Counts
GFP
LN+OHT
LN
HN+OHT
HN
Median of GFP
TNERT+OHT
TNERT
TNERT HIGH+OHT
TNERT HIGH
TNERT LOW+OHT
TNERT LOW
B
SL
r=0.69
SL+PD
r=0.59
SL
r=0.71
SL+PD
r=0.80
NANOG
FGFR1
FGFR2
C
10% LN
10% HN
HN
LN
-ve C
D
TNERTNBR1-/-
NBR2
Fgfr2 NBR1 -/-
Randomly integrated
EF1-α
Nanog
ERT2
SA-IRES
β-GeoR
Endogenous Nanog loci
eGFP-pA
E
TNERTNBR2-/-
NBR1
Fgfr2 NBR2 -/-
NANOG
Flag tag
Exon (Coding)
Avidin tag
Poly A
Exon (Non-coding)
F
TNERT
TNERTNBR1-/-
TNERTNBR2-/-
+OHT
-OHT
TNERT+OHT
TNERT
TNERT NBR1-/-+OHT
TNERT NBR1-/-
TNERT NBR2-/-+OHT
TNERT NBR2-/-
G
MEK1/2
pERK
NANOG
Nanog
FGFR2
Fgfr2
NONO
FGFBP1
NANOG low cell
NANOG high cell

Figure 5

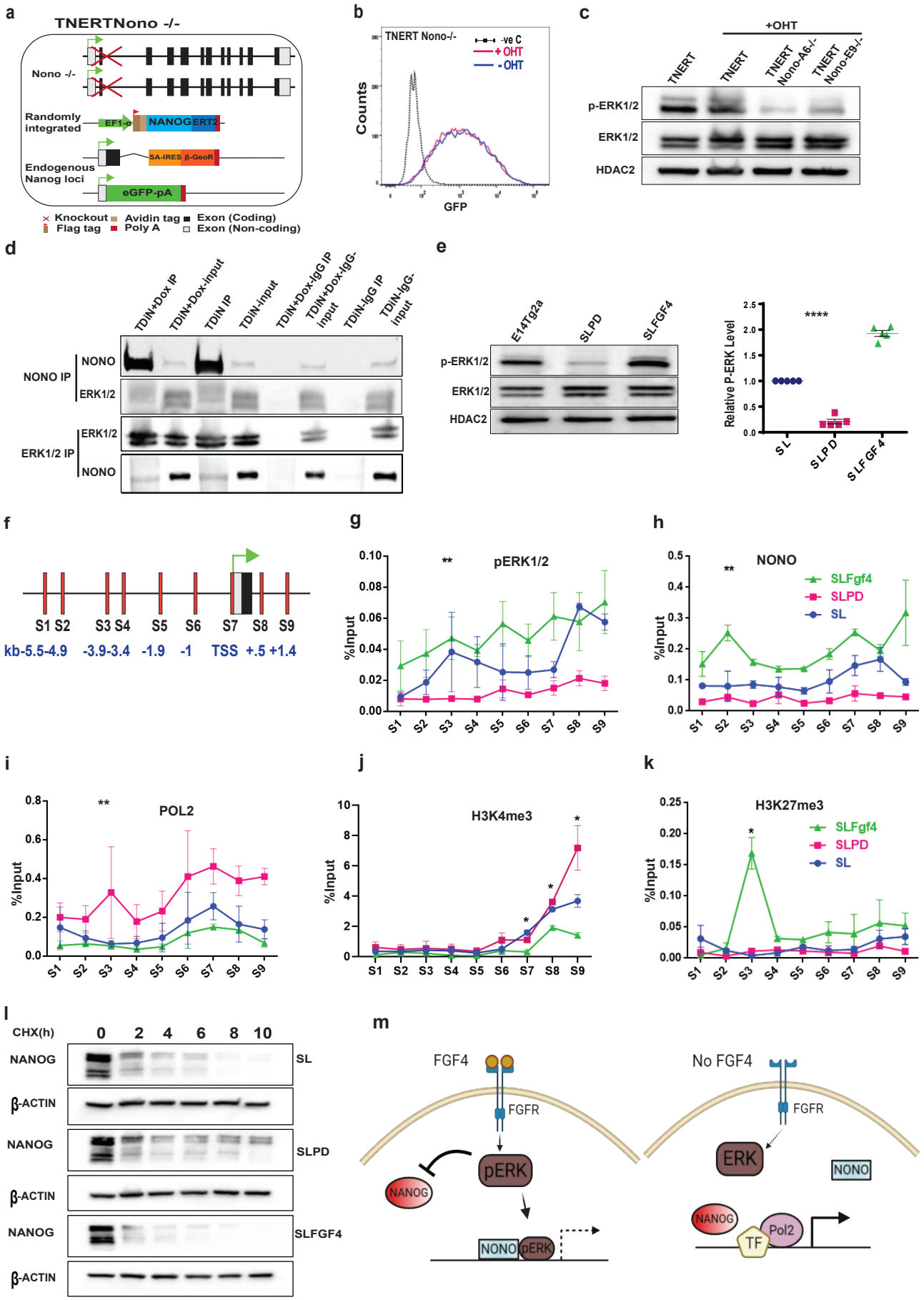
a
TNERTNono -/-
Nono -/-
Randomly integrated
EF1-α
NANOG
ERT2
Endogenous Nanog loci
SA-IRES
β-GeoR
eGFP-pA
Knockout
Avidin tag
Exon (Coding)
Flag tag
Poly A
Exon (Non-coding)
b
TNERT Nono-/-
-ve C
+ OHT
- OHT
Counts
GFP
c
+OHT
TNERT
TNERT
TNERT Nono-A6-/-
TNERT Nono-E9-/-
p-ERK1/2
ERK1/2
HDAC2
d
TDiN+Dox IP
TDiN+Dox-input
TDiN IP
TDiN-input
TDiN+Dox-IgG IP
TDiN+Dox-IgG-input
TDiN-IgG IP
TDiN-IgG-input
NONO IP
NONO
ERK1/2
ERK1/2 IP
ERK1/2
NONO
e
E14Tg2a
SLPD
SLFGF4
p-ERK1/2
ERK1/2
HDAC2
Relative P-ERK Level
****
SL
SLPD
SLFGF4
f
S1 S2 S3 S4 S5 S6 S7 S8 S9
kb-5.5-4.9 -3.9-3.4 -1.9 -1 TSS +.5 +1.4
g
pERK1/2
%Input
**
h
NONO
SLFgf4
SLPD
SL
i
POL2
j
H3K4me3
k
H3K27me3
l
CHX(h)
0 2 4 6 8 10
NANOG
β-ACTIN
SL
SLPD
SLFGF4
m
FGF4
FGFR
pERK
NANOG
NONO
pERK
No FGF4
FGFR
ERK
NONO
NANOG
TF
Pol2

Figure 6

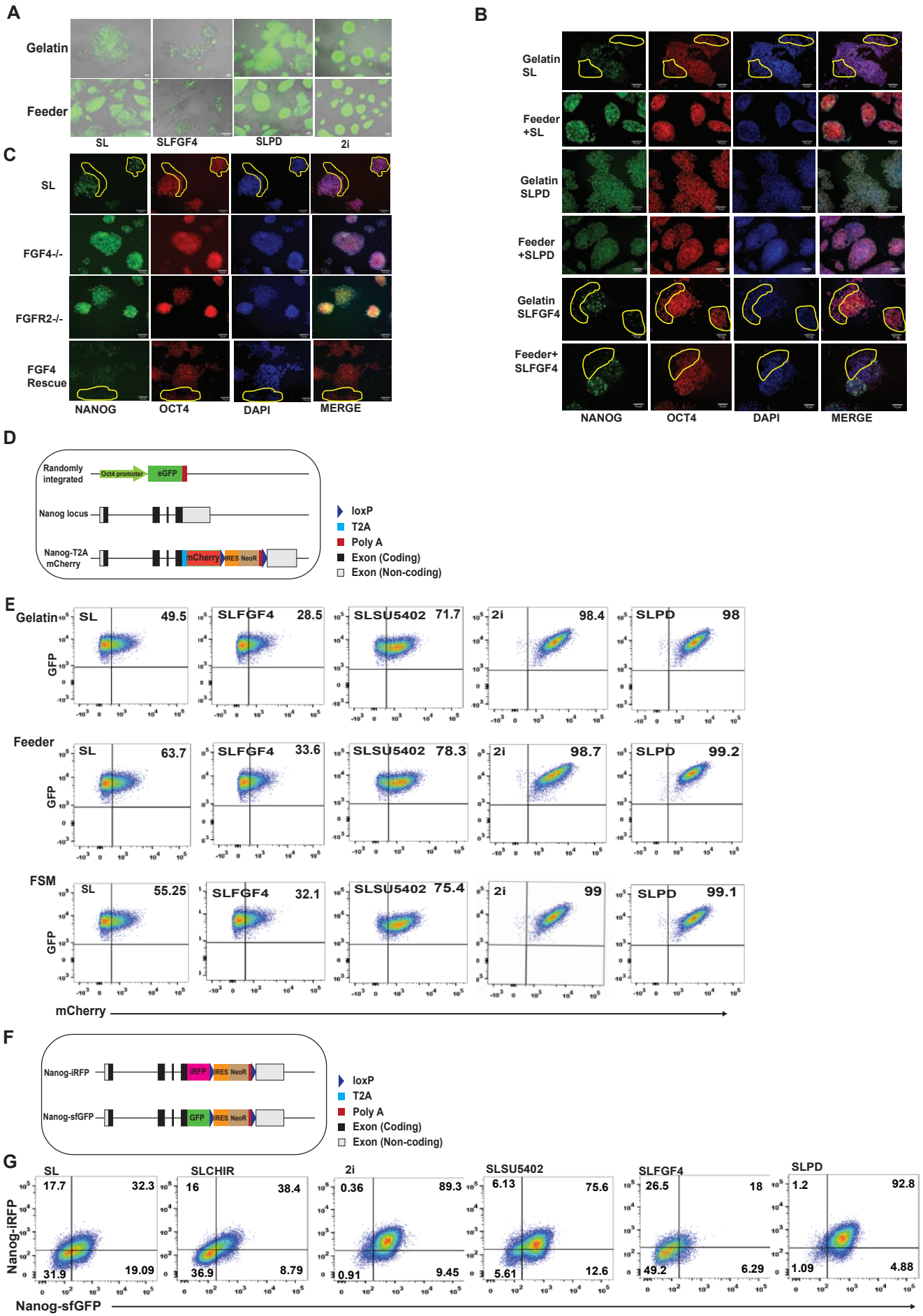
A
Gelatin
Feeder
SL
SLFGF4
SLPD
2i
B
Gelatin SL
Feeder +SL
Gelatin SLPD
Feeder +SLPD
Gelatin SLFGF4
Feeder+ SLFGF4
NANOG
OCT4
DAPI
MERGE
C
SL
FGF4-/-
FGFR2-/-
FGF4 Rescue
NANOG
OCT4
DAPI
MERGE
D
Randomly integrated
Oct4 promoter
eGFP
Nanog locus
Nanog-T2A mCherry
mCherry
IRES NeoR
loxP
T2A
Poly A
Exon (Coding)
Exon (Non-coding)
E
Gelatin
SL 49.5
SLFGF4 28.5
SLSU5402 71.7
2i 98.4
SLPD 98
Feeder
SL 63.7
SLFGF4 33.6
SLSU5402 78.3
2i 98.7
SLPD 99.2
FSM
SL 55.25
SLFGF4 32.1
SLSU5402 75.4
2i 99
SLPD 99.1
GFP
mCherry
F
Nanog-iRFP
iRFP
IRES NeoR
Nanog-sfGFP
GFP
loxP
T2A
Poly A
Exon (Coding)
Exon (Non-coding)
G
SL
17.7
32.3
31.9
19.09
SLCHIR
16
38.4
36.9
8.79
2i
0.36
89.3
0.91
9.45
SLSU5402
6.13
75.6
5.61
12.6
SLFGF4
26.5
18
49.2
6.29
SLPD
1.2
92.8
1.09
4.88
Nanog-iRFP
Nanog-sfGFP

Figure 7

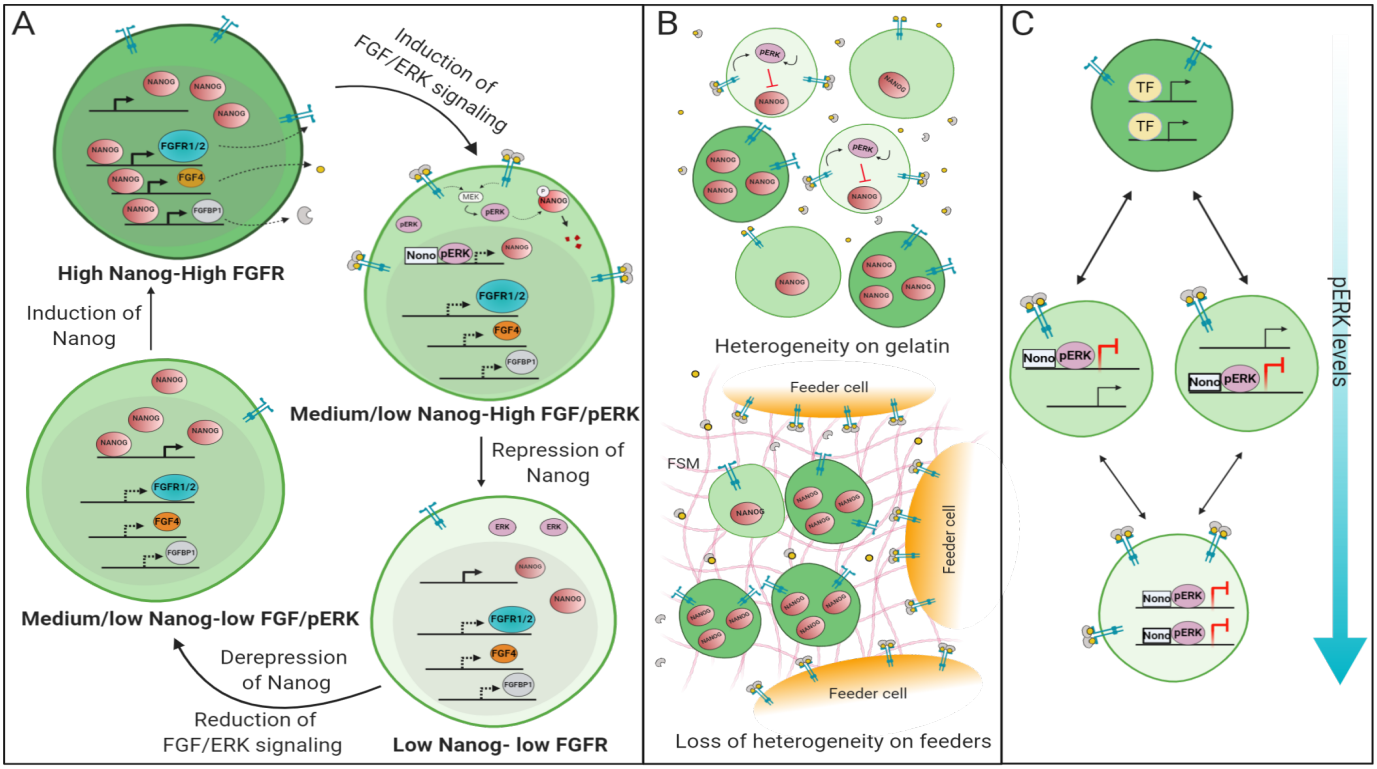
A
Induction of FGF/ERK signaling
High Nanog-High FGFR
Induction of Nanog
Medium/low Nanog-High FGF/pERK
Repression of Nanog
Medium/low Nanog-low FGF/pERK
Derepression of Nanog
Reduction of FGF/ERK signaling
Low Nanog- low FGFR
B
Heterogeneity on gelatin
Feeder cell
FSM
Feeder cell
Feeder cell
Loss of heterogeneity on feeders
C
TF
TF
pERK levels

KEY RESOURCES

REAGENT or RESOURCE	SOURCE	IDENTIFIER
Antibodies		
Anti-NANOG	Thermo Fisher Scientific	Cat# 14-5761-80, RRID: AB_763613
Anti-NANOG	Cell signaling Technology	Cat# 8822, RRID: AB_11217637
Nanog Polyclonal Antibody	Thermo Fisher Scientific	Cat# PA5-47376, RRID: AB_2607022
Anti-OCT3/4	Cell signaling Technology	Cat# 83932, RRID: AB_2721046
Anti-OCT3/4	Thermo Fisher Scientific	Cat# 14-5841-82, RRID: AB_914301
Anti-SOX 2	Cell signaling Technology	Cat# AMAb91307, RRID: AB_2665892
Anti-FGFR2	Thermo Fisher Scientific	Cat# PA1-24763, RRID: AB_780623
Anti-FGFR2	R&D Systems	Cat# MAB6843, RRID: AB_2103395
Anti-FGFR1	Cell signaling Technology	Cat# 9740, RRID: AB_11178519
FGFBP1 Polyclonal Antibody	Thermo Fisher Scientific	Cat# PA5-77220, RRID: AB_2720947
Anti-FGF4	Thermo Fisher Scientific	Cat# PA5-20483, RRID: AB_11152903
Anti-ERK1/2	Cell signaling Technology	Cat# 9102, RRID: AB_330744
Anti-P-ERK1/2	Cell signaling Technology	Cat# 4370, RRID: AB_2315112
Anti-P-ERK1/2	Cell signaling Technology	Cat#9101, RRID: AB_331646
Anti-Trimethyl Histone H3(Lys4) (C42D8)	Cell signaling Technology	Cat# 9751, RRID: AB_2616028)
Anti-Trimethyl Histone H3(Lys27)	Merck Millipore	Cat# 07-449, RRID: AB_310624
Anti- β-ACTIN	Sigma-Aldrich	Cat# A2228, RRID: AB_476697
Anti-HDAC2	Thermo Fisher Scientific	Cat# 51-5100; RRID: AB_2533908
Anti-RNA polymerase II Antibody, clone CTD4H8	Merck Millipore	Cat# 05-623, RRID: AB_309852
Chemicals, Peptides, and Recombinant Proteins		
rhFGF4	R&D Systems	Cat# 7460-F4-025
rhFGFBP1	R&D Systems	Cat# 1593-FB-025
Human FGF4 recombinant protein	Thermo Fisher Scientific	Cat# PHG0154
Human BMP4 recombinant protein	Thermo Fisher Scientific	Cat# PHC9534
Human EGF recombinant protein	Thermo Fisher Scientific	Cat# 01-107
Human Insulin recombinant protein	Thermo Fisher Scientific	Cat# RP-10908
Human bFGF recombinant protein	Thermo Fisher Scientific	Cat# RP-8628
G418 disulfate salt	Sigma-Aldrich	Cat# A1720
Doxycycline Hyclate	Sigma-Aldrich	Cat# D9891

SU5402	Sigma-Aldrich	Cat# SML0443
PD0325901	Sigma-Aldrich	Cat# PZ0162
CHIR99021	Sigma-Aldrich	Cat# SML1046
(Z)-4-Hydroxytamoxifen	Sigma-Aldrich	Cat# H7904
LIF	Made in-house	
Heparan sulfate sodium salt	Sigma-Aldrich	Cat# H7640
o-Phenylenediamine dihydrochloride	Sigma-Aldrich	Cat# P8287
Deposited Data		
Experimental Models: Cell Lines		
E14Tg2a		Chambers et al., 2007
TNGA		Chambers et al., 2007
TβC44Cre6		Chambers et al., 2007
TNERT	This Study	
NiRFP2A	This Study	
TDiN	This Study	
OGNM	This Study	
EDiN	This Study	
NisGFPDiN	This Study	
NsGiR	This Study	
TNERTFgfr2-/-	This Study	
TNERTFgfr1-/-	This Study	
TNERTFgf4-/-	This Study	
TNERTFgfbp1-/-	This Study	
TNERTNBR1-/-	This Study	
TNERTNBR2-/-	This Study	
TNERTNono-/-	This Study	
E14Tg2aFgf4-/-	This Study	
E14Tg2aFgfr2-/-	This Study	
E14Tg2aFgf4OE	This Study	
Oligonucleotides		
Oligos used for sgRNA cloning, genotyping, qPCR – RTPCR and ChIP-PCR	Supplemental Table 1	
Recombinant DNA		
pU6-(BbsI)-CBh-Cas9-T2A-mCherry	Addgene 64324	(Weber et al., 2015)
Mouse Oct4-GFP GOF18 transgenic reporter	Addgene 60527	(Gafni et al., 2013)
Nanog iRFP670 Fusion Targeting vector	This Study	
Nanog sfGFP Fusion Targeting vector	This Study	
Nanog-2A-mCherry	Addgene 59995	(Faddah et al., 2013)
pEF6V5His-Fgf4	This Study	
PEF6NanogERT2	This Study	
PTripZ-FaNanog	This Study	
pU6-iRFP	This Study	
pU6-iRFP Sg-Fgf4	This Study	
pU6-iRFP Sg-Fgfr1	This Study	
pU6-iRFP Sg-Fgfr2	This Study	

pU6-iRFP Sg-Fgfbp1	This Study	
pU6-iRFP Sg-Zfp281	This Study	
pU6-iRFP Sg-Nono	This Study	
pU6-iRFP Sg-Fgfr2-NBR1	This Study	
pU6-iRFP Sg-Fgfr2-NBR2	This Study	
pU6-iRFP Sg-Nanog-Stop	This Study	
pMKiN	This Study	
Software and Algorithms		
ImageJ	ImageJ	RRID: SCR_003070
FlowJo	BD Bioscience	RRID: SCR_008520
Integrative genomics viewer	Broad Institute	RRID: SCR_011793
SDS	Applied Biosystems	RRID: SCR_015806
Image Lab	Bio-rad	RRID: SCR_014210
GraphPad Prism	GraphPad	RRID: SCR_002798
Other		
Pierce Protein A/G Magnetic beads	Thermo Fisher Scientific	Cat# 88803
BD LSR Fortessa	BD Bioscience	N/A
MoFLo XDP	Beckman Coulter	N/A
Gallios Flowcytometer	Beckman Coulter	N/A
Chemidoc MP imaging system	Bio-rad	
Zeiss Axio Observer	Zeiss	N/A

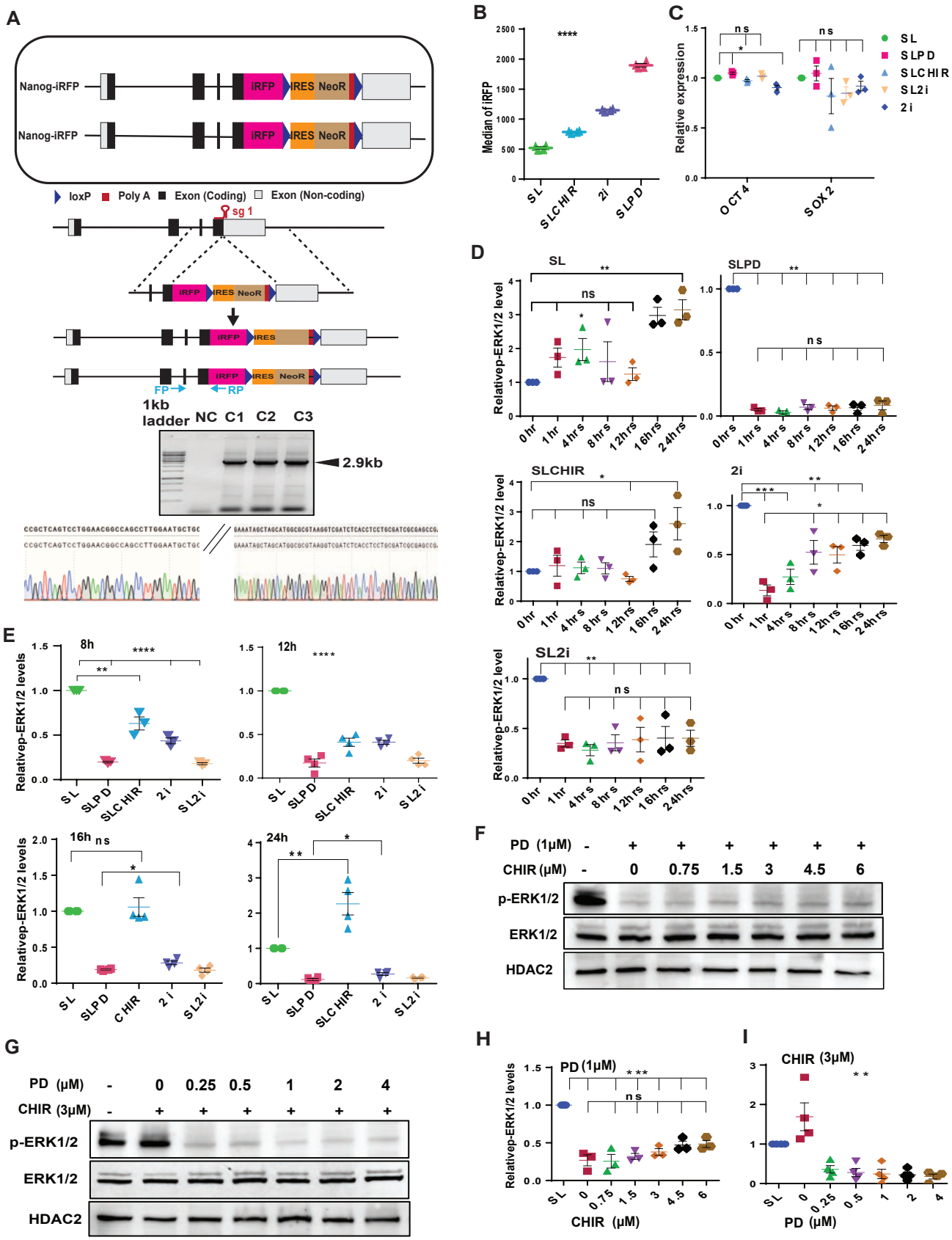
A
Nanog-iRFP
iRFP
IRES NeoR
loxP
Poly A
Exon (Coding)
Exon (Non-coding)
sg 1
FP
RP
1kb ladder
NC
C1
C2
C3
2.9kb
B
Median of iRFP
SL
SLCHIR
2i
SLPD
C
Relative expression
OCT4
SOX2
SL
SLPD
SLCHIR
SL2i
2i
D
Relativep-ERK1/2 level
SL
SLPD
SLCHIR
2i
SL2i
0hr
1hr
4hrs
8hrs
12hrs
16hrs
24hrs
E
Relativep-ERK1/2 levels
8h
12h
16h
24h
SL
SLPD
SLCHIR
2i
SL2i
F
PD (1μM)
CHIR (μM)
p-ERK1/2
ERK1/2
HDAC2
G
PD (μM)
CHIR (3μM)
p-ERK1/2
ERK1/2
HDAC2
H
PD (1μM)
Relativep-ERK1/2 levels
CHIR (μM)
I
CHIR (3μM)
PD (μM)

Supplemental data Fig 1: Residual MEK1/2 activity in the ground state prevents complete derepression of *Nanog.*

Related to Figure 1.

(A) (top) Schematic depiction of NiRFP2A with both alleles of *Nanog* fused to iRFP coding sequences in frame with last coding sequence. (middle) CRISPR mediated knock-in strategy of the iRFP-loxP-IRES-NeoR-loxP cassette into *Nanog* locus. The sgRNA includes the stop codon of the *Nanog* gene. The location of the genotyping primers (FP/RP) for the knock-in is marked by the arrows. (bottom) Genotyping of the NiRFP2A clones, a 2.9 kb band is amplified only in the knock-in clones as one of the primers is complementary to a sequence outside the left homology arm and the other primer is complementary to the iRFP sequence. (B) Relative quantification of the median of NANOG-iRFP population of NiRFP2A cells (n=4). (c) Relative quantification of OCT4 and SOX2. The expression is normalized relative to HDAC2 levels and expression levels of OCT4 and SOX2 in SL (n>=3). (D-E) Relative pERK1/2 expression levels in indicated time points and treatments (n=3). (F) Western blot of pERK1/2 and ERK1/2 in 1 μM PD and increasing concentrations of CHIR in SL media. (G) Western blot of pERK1/2 and ERK1/2 in 3 μM CHIR and increasing concentrations of PD in SL media. (H-I) Relative pERK1/2 expression levels in indicated concentrations of CHIR and PD respectively (n>=3). All error bars in the figure represent s.e.m.

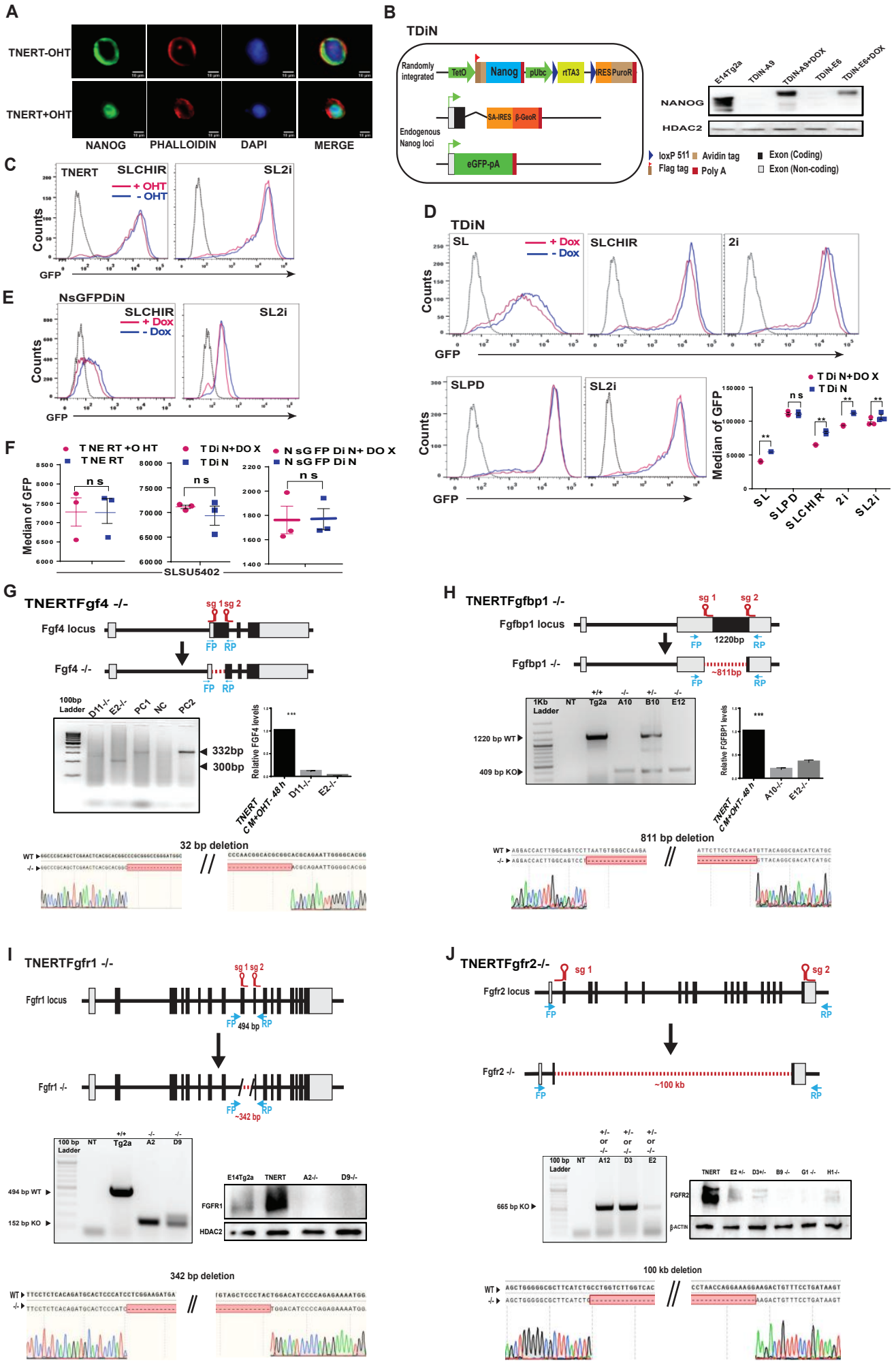
A
TNERT-OHT
TNERT+OHT
NANOG
PHALLOIDIN
DAPI
MERGE
B
TDiN
Randomly integrated
TetO
Nanog
pUbc
rtTA3
IRES PuroR
Endogenous Nanog loci
SA-IRES β-GeoR
eGFP-pA
E14Tg2a
TDiN-A9
TDiN-A9+DOX
TDiN-E6
TDiN-E6+DOX
NANOG
HDAC2
loxP 511
Avidin tag
Exon (Coding)
Flag tag
Poly A
Exon (Non-coding)
C
TNERT
SLCHIR
SL2i
+ OHT
- OHT
Counts
GFP
D
TDiN
SL
SLCHIR
2i
+ Dox
- Dox
SLPD
SL2i
Median of GFP
T Di N+DO X
T Di N
n s
SL
SLPD
SLCHIR
2i
SL2i
E
NsGFPDiN
SLCHIR
SL2i
+ Dox
- Dox
F
T NE RT +O HT
T NE RT
T Di N+DO X
T Di N
N sG FP Di N+ DO X
N sG FP Di N
SLSU5402
G
TNERTFgf4 -/-
sg 1 sg 2
Fgf4 locus
Fgf4 -/-
FP
RP
100bp Ladder
D11-/-
E2-/-
PC1
NC
PC2
332bp
300bp
Relative FGF4 levels
TNERT C M+OHT- 48 h
32 bp deletion
H
TNERTFgfbp1 -/-
sg 1
sg 2
Fgfbp1 locus
1220bp
Fgfbp1 -/-
~811bp
1Kb Ladder
NT
Tg2a
A10
B10
E12
1220 bp WT
409 bp KO
Relative FGFBP1 levels
811 bp deletion
I
TNERTFgfr1 -/-
sg 1 sg 2
Fgfr1 locus
494 bp
Fgfr1 -/-
~342 bp
100 bp Ladder
A2
D9
494 bp WT
152 bp KO
E14Tg2a
TNERT
A2-/-
D9-/-
FGFR1
HDAC2
342 bp deletion
J
TNERTFgfr2-/-
sg 1
sg 2
Fgfr2 locus
Fgfr2 -/-
~100 kb
A12
D3
E2
665 bp KO
FGFR2
β-ACTIN
100 kb deletion

Supplemental data Fig 2: FGF autocrine signaling pathway components are essential for *Nanog* autoregulation.

Related to Figure 2.

(A) Immunofluorescence of NANOG in TNERT cells after 30 mins treatment with or no OHT. Scale bars represent 10μM. (B) FACS profiles of TNERT treatment with or no OHT in SLCHIR and SL2i. (C) (left) Schematic of Doxycycline inducible TDiN cell line, generated by the introduction of a Tetracycline inducible Flag-Avi-NANOG (FaNANOG) transgene in Tβc44Cre6 cell line. (right) Western blot of FaNANOG in TDiN cells after 48 hrs treatment with or no Doxycycline. (D) FACS profiles of TDiN cell line in SL, SLCHIR, 2i, SL2i, and SLPD, (bottom right) *Nanog*:GFP population median of TDiN in indicated treatments (n=3). (E) FACS profiles of NsGFPDiN after 48 hrs of treatment with or no Doxycycline in SLCHIR and SL2i. (F) *Nanog*:GFP population median of TNERT, NsGFPDiN, and TDiN treated with SU5402, with OHT/Doxycycline or no OHT/Doxycycline. (G) (top) CRISPR-based knock-out strategy using paired sgRNA to knock-out *Fgf4* in TNERT. The sgRNAs are positioned at the beginning and the near end of exon II. The deletion results in the loss of the start codon and a part of the coding region in exon II. The dotted line represents the deleted region of the gene. FP and RP represent the relative positions of the genotyping primers. (middle left) genotyping PCR of TNERTFgf4-/- clones. The WT allele gives an amplicon of 332 bp and the knock-out allele a smaller amplicon by 32 bps or more. (middle right) The relative abundance of FGF4 in media of TNERT and TNERTFgf4-/- clones 48 hrs after OHT treatment. (bottom) Chromatogram of the TNERTFgf4-/- clones showing the sequences at the junction of the deletion. (H) (top) Schematic of the gene structure of *Fgfbp1* and the relative positions of the two sgRNAs used for paired sgRNA knock-out strategy. One sgRNA is complimentary to 5'UTR and the other to the 3' end of the coding region of the only exon. (middle left) Genotyping PCR showing a WT amplicon of 1220 bps and an amplicon around 400 bps in case of deletion. (middle right) The relative abundance of FGFFBP1 in media of TNERT and TNERTFgfbp1-/- clones 48 hrs after OHT treatment. (bottom) Chromatogram of the TNERTFgbp1-/- clone showing the sequences at the junction of the deletion. (I) Strategy for knock-out of *Fgfr1* in TNERT cells. The schematic depicts the gene structure of *Fgfr1* with the relative positions of the two sgRNAs. One sgRNA targets the 3'end of Intron 8 and the other exon10. (middle left) Genotyping PCR shows a WT allele amplicon at 494 bp and a knock-out allele with smaller amplicons around 150 bp. (middle right) Western blot analysis of FGFR1 in TNERT and TNERTFgfr1-/- clones. (bottom) chromatogram showing

the sequence of the deleted region (J) A paired sgRNA strategy to knock-out *Fgfr2* in TNERT. (top) The schematic represents the *Fgfr2* gene structure, with relative positions of the sgRNAs. One sgRNA target exon2 and the other sgRNA targets the coding region of the last exon approximately 100 kb apart. The dotted line represents the region of deletion in the *Fgfr2* gene. (middle left) PCR genotyping shows a 665 bp amplicon when at least one allele of *Fgfr2* is deleted. This genotyping strategy cannot distinguish between +/- and -/- genotypes. (middle right) Western blot analysis of FGFR2 protein in the Fgfr2 targeted clones distinguishing the +/- and -/- clones. (bottom) chromatogram represents the sequence of the genotyping amplicon indicating the exact sites of deletion. All error bars in the figure represent s.e.m.

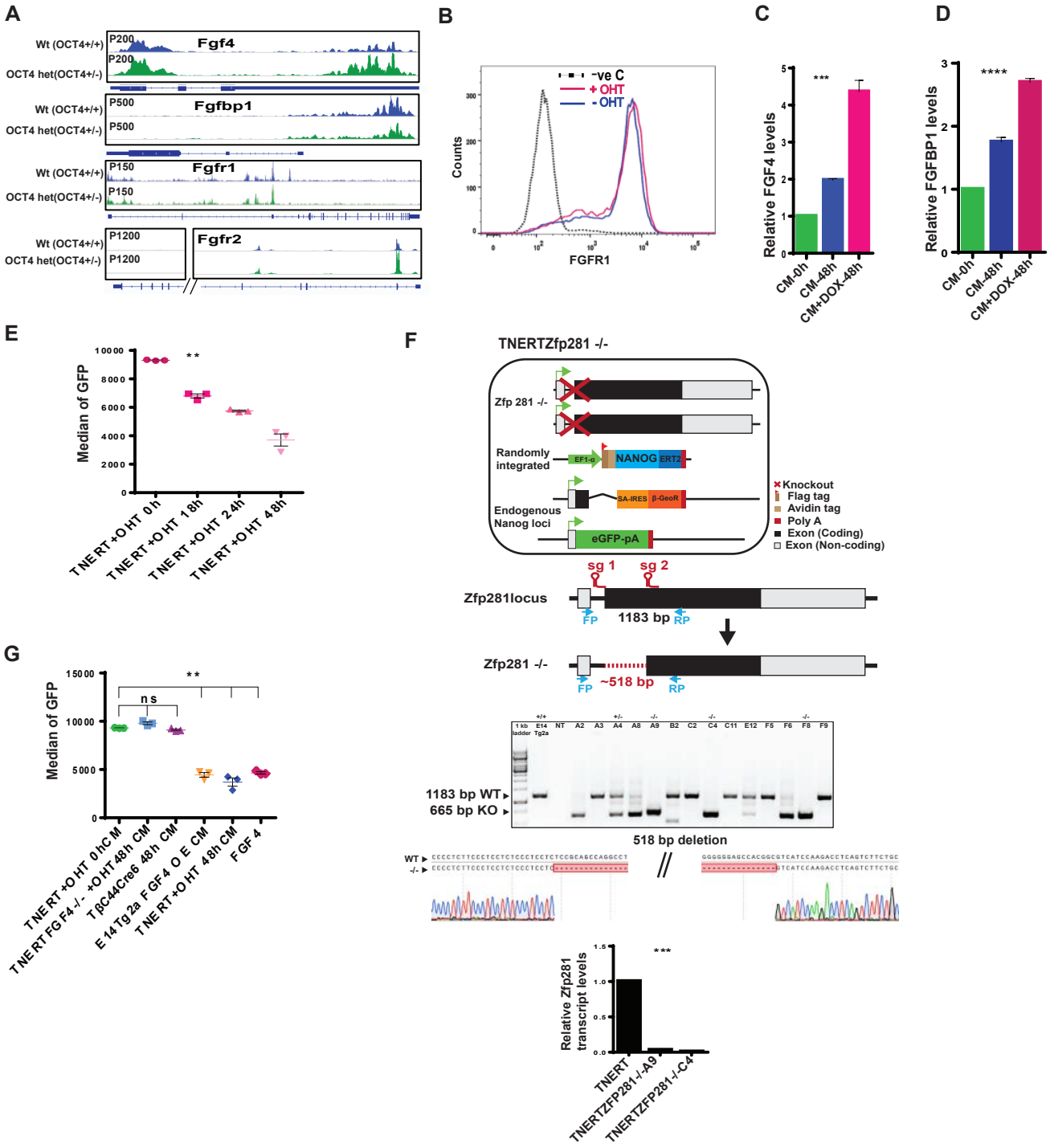
A
Wt (OCT4+/+)
OCT4 het(OCT4+/-)
Fgf4
Fgfbp1
Fgfr1
Fgfr2
B
-ve C
+OHT
-OHT
Counts
FGFR1
C
Relative FGF4 levels
CM-0h
CM-48h
CM+DOX-48h
D
Relative FGFBP1 levels
E
Median of GFP
TNERT+OHT 0h
TNERT+OHT 18h
TNERT+OHT 24h
TNERT+OHT 48h
F
TNERTZfp281 -/-
Zfp 281 -/-
Randomly integrated
NANOG
ERT2
Endogenous Nanog loci
eGFP-pA
Knockout
Flag tag
Avidin tag
Poly A
Exon (Coding)
Exon (Non-coding)
sg 1
sg 2
Zfp281locus
FP
1183 bp
RP
Zfp281 -/-
~518 bp
1183 bp WT
665 bp KO
518 bp deletion
Relative Zfp281 transcript levels
TNERT
TNERTZFP281-/-A9
TNERTZFP281-/-C4
G
Median of GFP
ns
TNERT+OHT 0hCM
TNERTFG F4-/- +OHT 48h CM
TβC44Cre6 48h CM
E14Tg2a FGF4 O E CM
TNERT+OHT 48h CM
FGF4
H
Relative FGF4 levels
CM-0h
CM-18h
CM+OHT-18h
CM-24h
CM+OHT-24h
CM-48h
CM+OHT-48h
I
Relative FGFBP1 levels
J
Relative FGF4 levels
TNERT+OHTCM-0h
TNERTFgf4-/- CM
TNERTCM-48h
E14Tg2aFgf4 O.E.CM
TNERTCM+OHT-48h
FGF4
K
Relative FGFBP1 levels
TNERTFgfbp1-/- +OHT CM
FGFBP1

Supplemental data Fig 3: *Nanog* enhances expression of FGF autocrine signaling pathway components.

Related to Figure 3.

(A) Browser tracks of NANOG enrichment in Fragment Per Kilobase of transcripts per Million (FPKM) in Oct4+/+ cells (normal NANOG levels) and Oct4+/- cells (higher NANOG levels) (Karwacki-Neisius et al., 2013) at *Fgf4, Fgfbp1, Fgfr1,* and *Fgfr2* loci. (B) Histogram of FGFR1 expression on the cell surface analyzed by immunostaining and FACS of fixed but unpermeabilized TNERT cells treated with (red) or no OHT (blue). (C-D) ELISA-based relative quantification of FGF4 and FGFBP1in media from EDiN cells cultured with or no Doxycycline (n=3). EDiN cell was generated by introducing a Doxycycline inducible Flag-Avi-NANOG transgene in E14Tg2a cells. (E) *Nanog*:GFP population median of Tβc44Cre6 treated with OHT induced conditioned media collected after different time points (n=3). (F) (top) Schematic of TNERTZfp281-/- cells, (upper-middle) CRISPR based paired guide knock-out strategy indicating the relative position of the sgRNAs, FP and RP indicate the genotyping primers. (lower middle) Genotyping PCR indicating +/- and -/- clones. (bottom) The sequencing chromatogram of the deleted region confirms the exact site of deletion, followed by RT-qPCR analysis of the *Zfp281* transcripts. (G) *Nanog*:GFP population median of Tβc44Cre6 treated with conditioned media from TNERT+OHT 0 hrs, TNERTFGF4-/- +OHT 48 hrs, Tβc44Cre6 48 hrs, E14Tg2a-FGF4-OE (overexpression) 48 hrs, TNERT+OHT 48 hrs and 50ng/ml FGF4 (n=3). (H-I) ELISA-based relative quantities of FGF4 and FGFBP1 in media from TNERT after 18, 24, and 48 hrs of OHT treatment (n=3). (J) ELISA-based relative quantities of FGF4 in conditioned media from cell lines -TNERT+ OHT 0 hrs, TNERTFGF4-/- + OHT 48 hrs, E14Tg2a-FGF4-OE 48 hrs (overexpression), TNERT-/+OHT 48 hrs, and 50ng/ml FGF4 (n=3). (K) ELISA-based relative quantities of FGFBP1 in conditioned media from various cell lines - TNERT+ OHT 0 hrs, TNERT-Fgfbp1-/- 48 hrs +OHT, TNERT 48 hrs -/+ OHT, and 50 ng/ml FGBP1 (n=3). All error bars in the figure represent s.e.m.

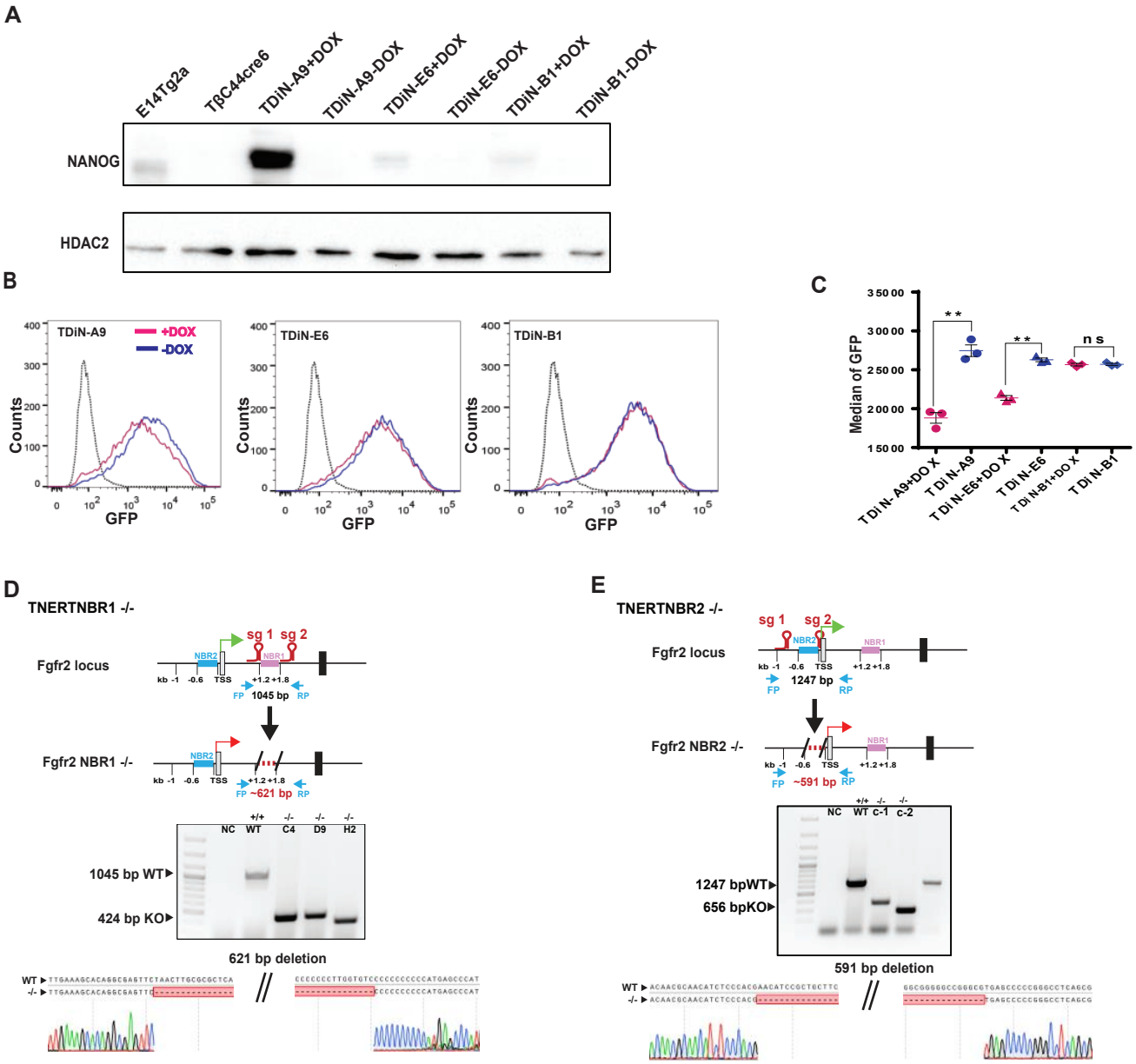
A
E14Tg2a
TβC44cre6
TDiN-A9+DOX
TDiN-A9-DOX
TDiN-E6+DOX
TDiN-E6-DOX
TDiN-B1+DOX
TDiN-B1-DOX
NANOG
HDAC2
B
TDiN-A9
+DOX
-DOX
TDiN-E6
TDiN-B1
Counts
GFP
C
Median of GFP
**
**
n s
TDiN-A9+DOX
TDiN-A9
TDiN-E6+DOX
TDiN-E6
TDiN-B1+DOX
TDiN-B1
D
TNERTNBR1 -/-
Fgfr2 locus
sg 1
sg 2
NBR2
NBR1
TSS
1045 bp
FP
RP
Fgfr2 NBR1 -/-
~621 bp
NC
WT
C4
D9
H2
1045 bp WT
424 bp KO
621 bp deletion
WT
-/-
E
TNERTNBR2 -/-
Fgfr2 locus
1247 bp
Fgfr2 NBR2 -/-
~591 bp
c-1
c-2
1247 bpWT
656 bpKO
591 bp deletion

Supplemental data Fig 4: NANOG induced FGFR2 triggers autoregulation predominately in the ES cell population with higher *Nanog* expression.

Related to Figure 4.

(A) Western blot analysis of Flag-Avi-NANOG in different clones of TDiN treated with or no Doxycycline showing different levels of NANOG expression relative to E14Tg2a. The clones show different levels of expression Flag- Avi-NANOG upon Doxycycline treatment. (B) FACS profiles of *Nanog*:GFP in TDiN clones treated with or no Doxycycline (C) *Nanog*:GFP population median of TDiN clones (n=3). (D)(top) Schematic of strategy for deletion of NANOG Binding Region 1 (NBR1) in TNERT indicating the position of the NBR1 and the relative position of the sgRNA pair. The sgRNAs are complementary to sequences around 1.2 kb and 1.8 kb downstream of TSS. FP and RP indicate the relative position of the primers for genotyping. (middle) Genotyping of TNERT NBR1 knock-out clones. The WT shows an amplicon of 1045 bp, upon deletion around 600 bp sequence comprising multiple NANOG binding sites is deleted. (bottom) Sequence and chromatogram of the genotype PCR amplicon indicating the exact sequence of the junction of deletion in TNERTNBR1-/- clone. (E) Schematic of strategy for deletion of NANOG Binding Region 2 (NBR2) in TNERT indicating the position of NBR2 and relative position of the sgRNA pair. The sgRNAs are complementary to sequences around TSS and 0.6 kb upstream of TSS of *Fgfr2*. (middle) Genotyping of the TNERTNBR2 knock-out clones. The WT shows an amplicon of 1247 bp. The knock-out would lead to deletion of around 690 bps and a smaller amplicon of around 650 bps. (bottom) Sequence and chromatogram of the PCR amplicon from TNERT knock-out clones showing the exact site of deletion in TNERT NBR2-/- clone. All error bars in the figure represent s.e.m.

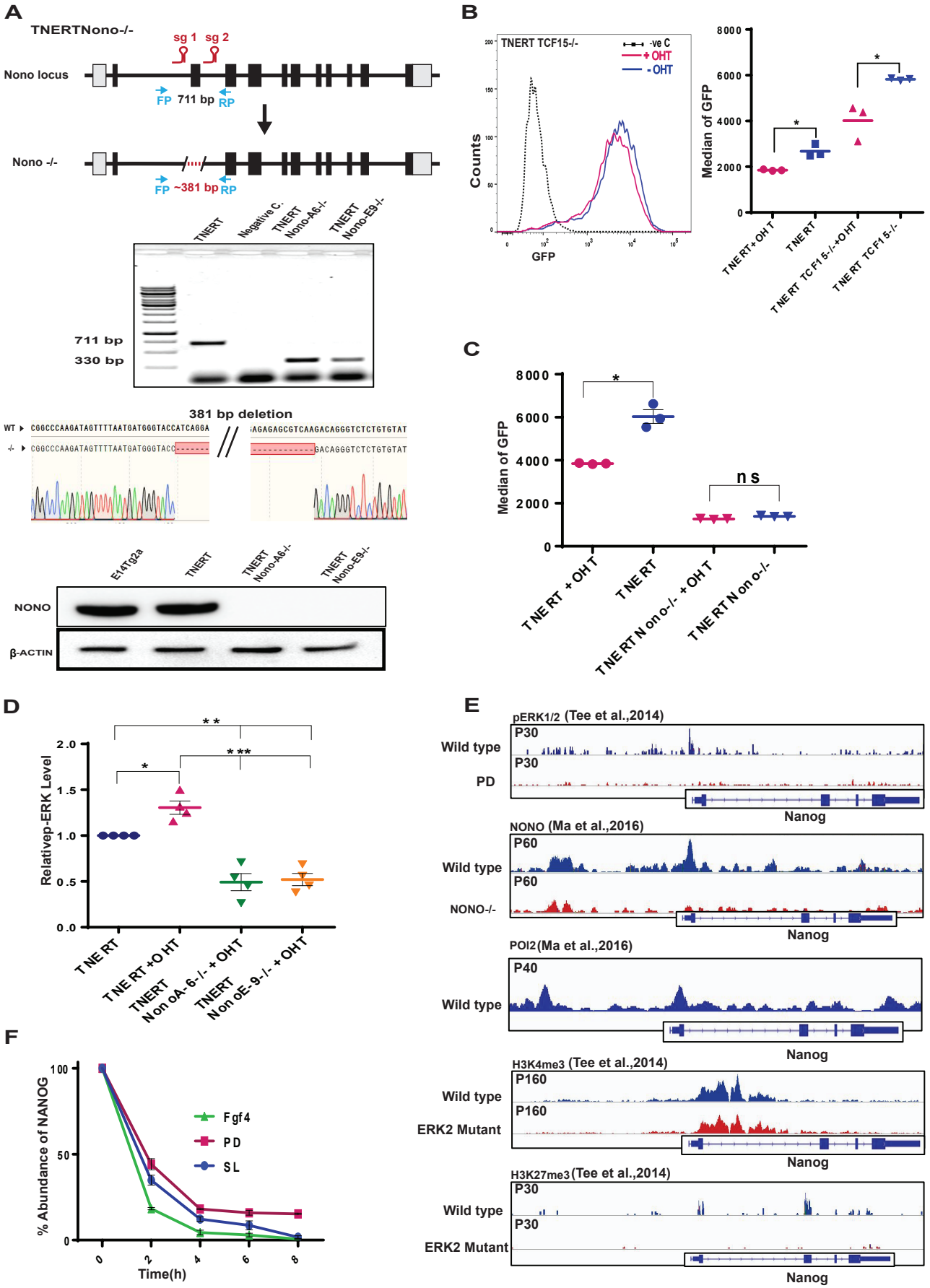
A
TNERTNono-/-
sg 1
sg 2
Nono locus
FP
711 bp
RP
Nono -/-
FP
~381 bp
RP
TNERT
Negative C.
TNERT Nono-A6-/-
TNERT Nono-E9-/-
711 bp
330 bp
381 bp deletion
WT
-/-
E14Tg2a
TNERT
TNERT Nono-A6-/-
TNERT Nono-E9-/-
NONO
β-ACTIN
B
TNERT TCF15-/-
-ve C
+ OHT
- OHT
Counts
GFP
Median of GFP
TNERT+OHT
TNERT
TNERT TCF15-/-+OHT
TNERT TCF15-/-
C
Median of GFP
n s
TNERT + OHT
TNERT
TNERT Nono-/- + OHT
TNERT Nono-/-
D
Relativep-ERK Level
TNERT
TNERT +OHT
TNERT Nono A-6-/- + OHT
TNERT Nono E-9-/- + OHT
E
pERK1/2 (Tee et al.,2014)
Wild type
PD
P30
Nanog
NONO (Ma et al.,2016)
Wild type
NONO-/-
P60
POI2 (Ma et al.,2016)
P40
H3K4me3 (Tee et al.,2014)
ERK2 Mutant
P160
H3K27me3 (Tee et al.,2014)
F
% Abundance of NANOG
Fgf4
PD
SL
Time(h)

Supplemental data Fig 5: ERK1/2 interacts and recruits NONO to repress *Nanog* transcription.

Related to Figure 5.

(A) A CRISPR-based knock-out strategy using paired sgRNA, to knock-out of *Nono* in TNERT cells. (top) The schematic represents the mouse *Nono* gene structure with relative positions of the two sgRNAs flanking the second coding exon of *Nono*. FP and RP indicate the relative position of genotyping primers. The dotted line indicates the region of deletion in the *Nono* gene. (middle) Genotyping PCR of the *Nono*-/- deletion in TNERT. The WT allele gave an amplicon of 711 bp and the deleted allele shows a smaller amplicon of 330 bp; followed by sequence and chromatogram indicating the deletion site (bottom) Western blot analysis of NONO protein in TNERT and TNERTNono-/- clones. **(B)** FACS profiles of TNERTTcf15-/- cells, treated with OHT (red) or no OHT (blue). (Right) Nanog:GFP population median of TNERTTcf15-/- cells (n=3). **(C)** *Nanog*:GFP population median of TNERT and TNERTNono-/- treated with or no OHT (n=3). **(D)** The relative abundance of pERK1/2 in TNERT treated with or no OHT and TNERTNono-/- with OHT (n=4). **(E)** Browser tracks of pERK1/2, NONO, POL2, H3K4me3, H3K27me3 enrichment in Fragment Per Kilobase of transcripts per Million (FPKM) on *Nanog* gene (Ma et al., 2016; Tee et al., 2014) **(F)** The relative abundance of NANOG after 0, 2, 4, 6, and 8 hrs of Cycloheximide (CHX) chase cultured in SL, PD, and FGF4 (n=3). All error bars in the figure represent s.e.m.

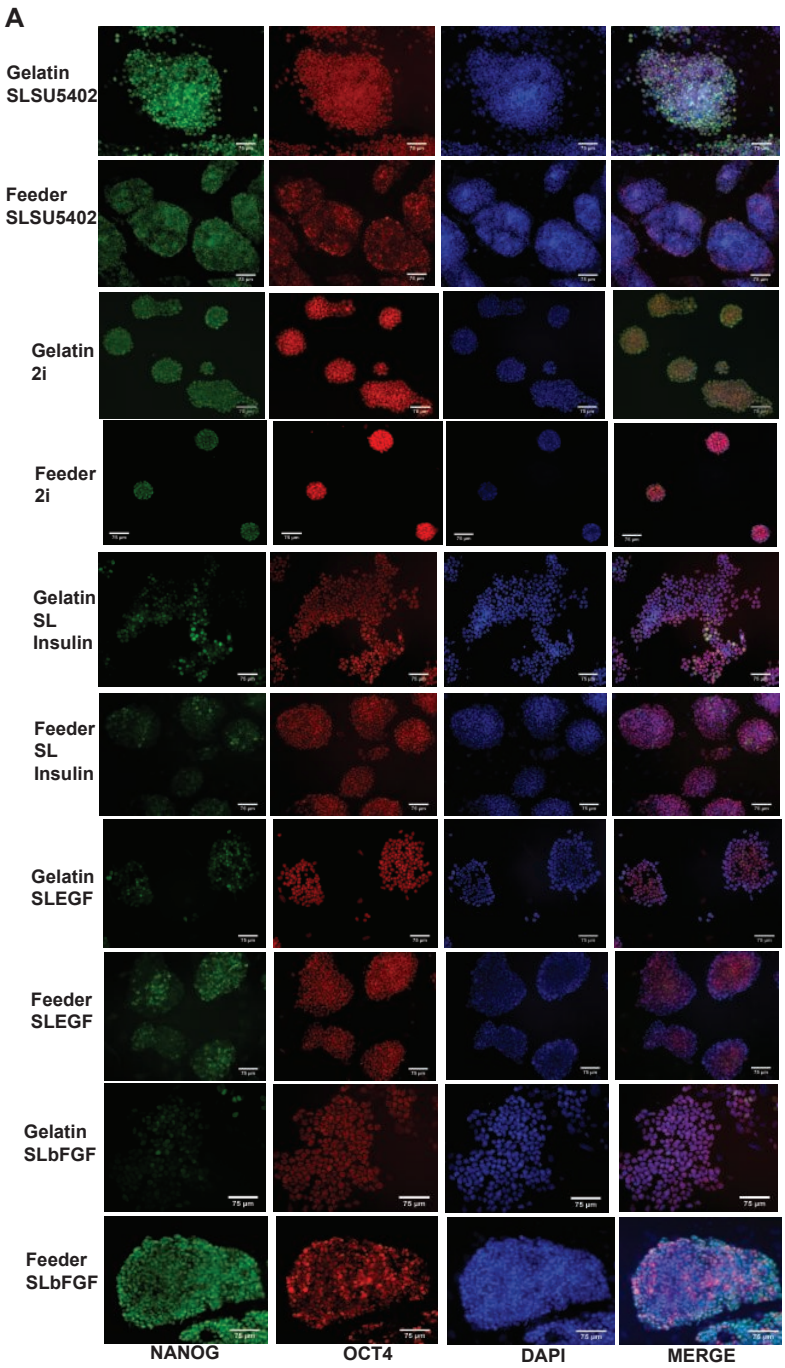
A
Gelatin SLSU5402
Feeder SLSU5402
Gelatin 2i
Feeder 2i
Gelatin SL Insulin
Feeder SL Insulin
Gelatin SLEGF
Feeder SLEGF
Gelatin SLbFGF
Feeder SLbFGF
NANOG
OCT4
DAPI
MERGE

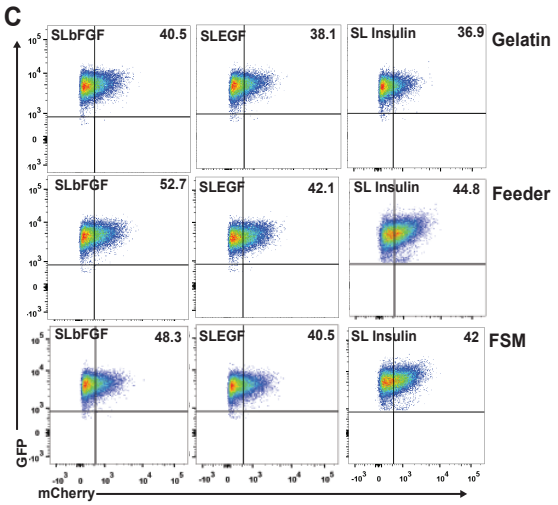
C
SLbFGF 40.5
SLEGF 38.1
SL Insulin 36.9
Gelatin
SLbFGF 52.7
SLEGF 42.1
SL Insulin 44.8
Feeder
SLbFGF 48.3
SLEGF 40.5
SL Insulin 42
FSM
GFP
mCherry

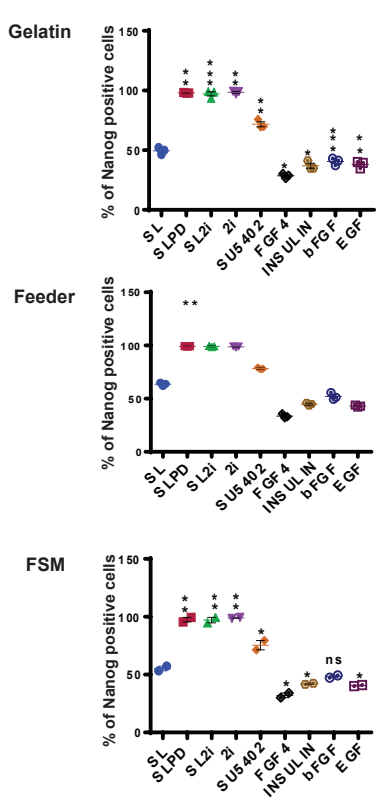
D
Gelatin
Feeder
FSM
% of Nanog positive cells
SL
SLPD
SL2i
2i
SU5402
FGF4
INSULIN
bFGF
EGF
ns

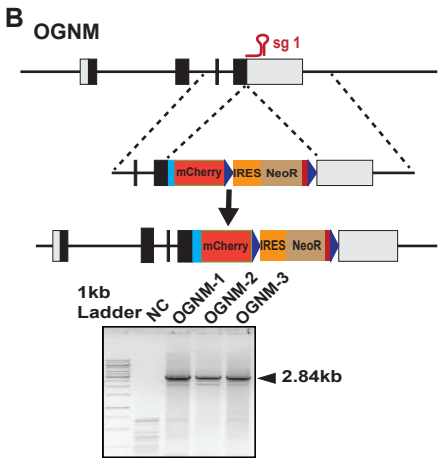
B
OGNM
sg 1
mCherry
IRES NeoR
1kb Ladder
NC
OGNM-1
OGNM-2
OGNM-3
2.84kb

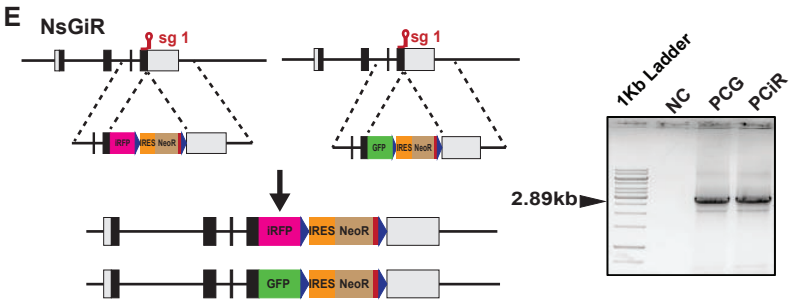
E
NsGiR
sg 1
iRFP
IRES NeoR
GFP
1Kb Ladder
NC
PCG
PCiR
2.89kb

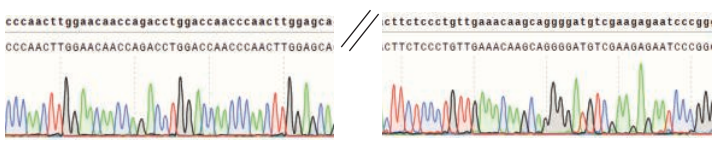

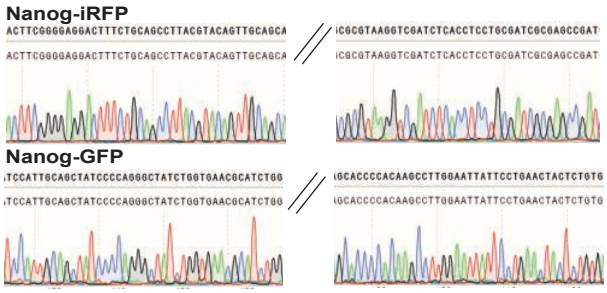
Nanog-iRFP
Nanog-GFP

Supplemental data Fig 6: FGF autocrine signaling regulates *Nanog* heterogeneity and monoallelic expression.

Related to Figure 6.

(A) Immunofluorescence of NANOG and OCT4 in E14Tg2a cells cultured on gelatin or feeders in SLSU5402, 2i, SLInsulin, SLEGF, and SLbFGF. Scale bars represent 75μM. (B) (top) Schematic of Knock-in of a T2AmCherry-loxP-IRESNeo-loxP cassette in frame with the last coding sequence of the last exon of *Nanog* in an *Oct4*-GFP cell line to generate OGNM cell line. The OGNM cell line will produce a T2A-mcherry protein from the knock-in allele and the *Oct4* expression is reported by an Oct4-GFP transgenic reporter (addgene:60527) randomly integrated into the genome. (middle) Genotyping PCR using one primer from the mCherry cassette and the other from a sequence complementary to the sequence outside the homology arms. (bottom) Chromatogram of the *Nanog*-T2AmCherry junction in the knock-in cells showing the Nanog coding sequences in frame with T2AmCherry sequence. (C) FACS profiles of OGNM cultured in SLbFGF, SLEGF, and SLInsulin on gelatin, feeders, and Feeder Secreted Matrix (FSM). (D) Percentage of *Nanog*-T2AmCherry expressing cells in indicated conditions cultured on gelatin (n=3) (top), feeder (n=3) (middle), and feeder secreted matrix (n=2) (bottom) (E) (top) Schematic of the strategy of generating NsGiR cell line. iRFP-loxP-IRESNeo-loxP is knocked-in in frame with the last coding sequence of *Nanog* in one allele and sfGFP-loxP-IRESNeo-loxP cassette into another allele. (middle) PCR genotyping of knock-in of iRFP-loxP-IRESNeo-loxP and sfGFP-loxP-IRESNeo-loxP into different alleles of *Nanog*. (bottom) Chromatogram of the PCR genotyping amplicons showing the junction of *Nanog* coding sequence with the iRFP670 or sfGFP sequences.

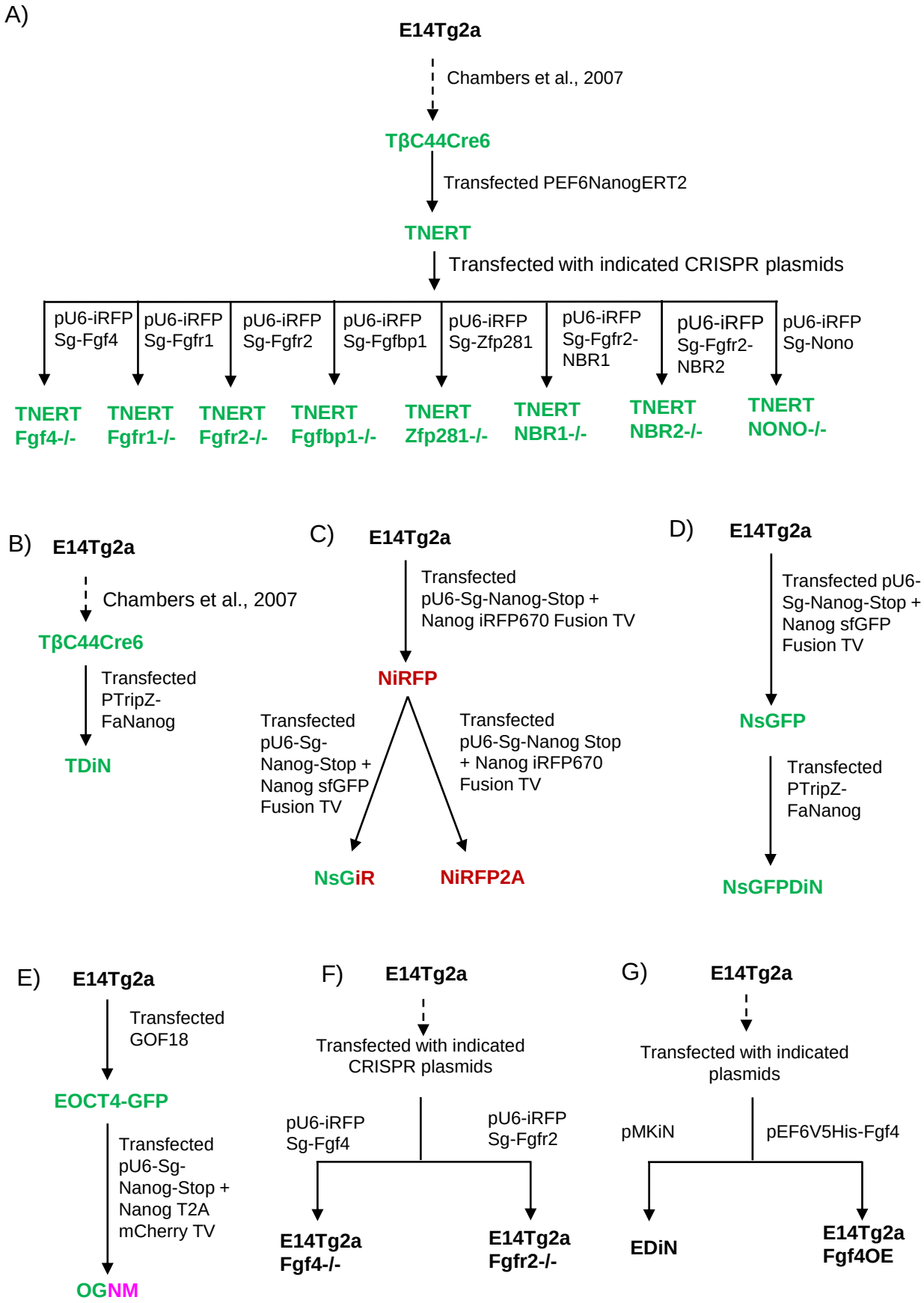
A)
E14Tg2a
Chambers et al., 2007
TβC44Cre6
Transfected PEF6NanogERT2
TNERT
Transfected with indicated CRISPR plasmids
pU6-iRFP Sg-Fgf4
pU6-iRFP Sg-Fgfr1
pU6-iRFP Sg-Fgfr2
pU6-iRFP Sg-Fgfbp1
pU6-iRFP Sg-Zfp281
pU6-iRFP Sg-Fgfr2-NBR1
pU6-iRFP Sg-Fgfr2-NBR2
pU6-iRFP Sg-Nono
TNERT Fgf4-/-
TNERT Fgfr1-/-
TNERT Fgfr2-/-
TNERT Fgfbp1-/-
TNERT Zfp281-/-
TNERT NBR1-/-
TNERT NBR2-/-
TNERT NONO-/-
B)
E14Tg2a
Chambers et al., 2007
TβC44Cre6
Transfected PTripZ-FaNanog
TDiN
C)
E14Tg2a
Transfected pU6-Sg-Nanog-Stop + Nanog iRFP670 Fusion TV
NiRFP
Transfected pU6-Sg-Nanog-Stop + Nanog sfGFP Fusion TV
Transfected pU6-Sg-Nanog Stop + Nanog iRFP670 Fusion TV
NsGiR
NiRFP2A
D)
E14Tg2a
Transfected pU6-Sg-Nanog-Stop + Nanog sfGFP Fusion TV
NsGFP
Transfected PTripZ-FaNanog
NsGFPDiN
E)
E14Tg2a
Transfected GOF18
EOCT4-GFP
Transfected pU6-Sg-Nanog-Stop + Nanog T2A mCherry TV
OGNM
F)
E14Tg2a
Transfected with indicated CRISPR plasmids
pU6-iRFP Sg-Fgf4
pU6-iRFP Sg-Fgfr2
E14Tg2a Fgf4-/-
E14Tg2a Fgfr2-/-
G)
E14Tg2a
Transfected with indicated plasmids
pMKiN
pEF6V5His-Fgf4
EDiN
E14Tg2a Fgf4OE

Supplemental data Fig 7: A pedigree chart of cell lines used in this study.

Related to STAR methods.

(A) A flow chart illustarting the lineage and process of generation of TNERT and generation of knock out cells lines in TNERT background. (B) A flow chart describing derivation of TDiN. (C) A flow chart depicting derivation of NsGiR and NiRFP2A from E14Tg2a. (D) A flow chart describing derivation of NsGFPDiN from E14Tg2a. (E) (D) A flow chart describing derivation of OGNM from E14Tg2a. (F) a flowchart depicting derivation of Fgf4-/- and Fgfr2-/- ES cell lines from E14Tg2a. (G) a flowchart depicting derivation of EDiN and Fgf4OE (over expression) ES cell lines from E14Tg2a.

Supplemental Table 1. List of oligonucleotides used in the study

Name of the Oligo	Sequence
Oligos for paired sgRNA Knock-out	
Fgf4 sgRNA1	CACCGCCGTGCGTGAGTTCGAGCTG
	AAACCAGCTCGAACTCACGCACGGG
Fgf4 sgRNA2	CACCGCGAAACGCGGGCCGACCAC
	AAACGTGGTCGGCCCGCGTTTCGC
Fgfr1 sgRNA1	CACCGCGTCATCATCTTCCGAGGAT
	AAACATCCTCGGAAGATGATGACGC
Fgfr1 sgRNA2	CACCGTTCTCTGGGGATGTCCAGTA
	AAACTACTGGACATCCCCAGAGAAC
Fgfr2 sgRNA1	CACCGCTGGGGGCGCTTCATCTGCC
	AAACGGCAGATGAAGCGCCCCCAGG
Fgfr2 sgRNA2	CACCGCTCAGTGTAAGTAGGTTCC
	AAACGGAACCTACTTACACTGAGC
Fgfbp1 sgRNA1	CACCGCACAGTCTTGGCCCACATTA
	AAACTAATGTGGGCCAAGACTGTGC
Fgfbp1 sgRNA2	CACCGATGTCGCCTGTAACATGTTG
	AAACCAACATGTTACAGGCGACATC
Fgfr2 NBR1 sgRNA1	CACCGTCGGAGCAGCTAGGCGAACT
	AAACAGTTCGCCTAGCTGCTCCGAC
Fgfr2 NBR1 sgRNA2	CACCGTTGTGTTTAGGGCCCCCCCT
	AAACAGGGGGGGCCCTAAACACAAC
Fgfr2 NBR2 sgRNA1	CACCGTGGAAGCAGCGGATGTTCGT
	AAACACGAACATCCGCTGCTTCCAC
Fgfr2 NBR2 sgRNA2	CACCGACCGGAGCTGCTCTCGGATC
	AAACGATCCGAGAGCAGCTCCGGTC
Nanog -stop codon sgRNA	CACCGTATGAGACTTACGCAACATC
	AAACGATGTTGCGTAAGTCTCATAG
Zfp281 sgRNA1	CACCGAGGCCTGGCTGCGGAGAGG
	AAACCCTCTCCGCAGCCAGGCCTC
Zfp281 sgRNA1	CACCGCGGGGTATGAAAATCGGCAG
	AAACCTGCCGATTTTCATACCCCGG
Nono sgRNA1	CACCGTTTTAATGATGGGTACCATC
	AAACGATGGTACCCATCATTAAAAC
Nono sgRNA1	CACCGTTCCGAGAGAGCGTCAAGAC
	AAACGTCTTGACGCTCTCTCGGAAC
Genotyping primers	
Fgf4 knock-out	CGCAGCACTCACCGAACTCA
	TGCCCACGTTGCAGTAGAGC
Fgfr1 knock-out	GTCTAGACAGGGCGAATGCTGTTT
	ACTTGAACTTCACCGTCTTGGCAG
Fgfr2 knock-out	TCTGGGTTTAAGCAAGTTGGCACT
	CAGCATACATGGTGGGTCAGAGAG
Fgfbp1 knock-out	GAAAGTGAGAAGCTGAGTGAATGG
	TATATGCACCTAGGTTTGTGGTCC
Fgfr2 NBR1 knock-out	GAAGAAACTGCTGGAGTGTGGTCA
	AGGGTAGTTCCAGGATACCTCAGC
Fgfr2 NBR2 knock-out	AGAGGCTTTGGATGACTCTGCAAC
	GCGATGATCTCGGAGGAAAACTCC
Zfp281 knock-out	TGTGGAGAGGACGGCGTTATTTTT
	TGAAACCCATACTACACTGGCTGC
Nono Knock out	AGGTTTCCCTGCTTGTCTTTGTCT
	GCAGCAACGCCCTTAATTTCAACA

Nanog-iRFP670	ACCCAGGGGTGACAAAGTATTCCAA
	GCATTTTCCGTAATGCGCGTGATCC
Nanog-sfGFP	ACCCAGGGGTGACAAAGTATTCCAA
	CGTTTGTAGCATCACCTTCACCCTC
Nanog-T2AmCherry	ACCCAGGGGTGACAAAGTATTCCAA
	TCGCCCTTGCTCACCATTGGCCCG GGATTCTCTTC
q-RT-PCR primers	
Dusp6	CTGCCATTAATGTGGCCATCCC
	GTGTTCTCATTCCAGTCGCTGC
Nanog	TGGTCCCCACAGTTTGCCTAGTTC
	CAGGTCTTCAGAGGAAGGGCGA
Oct4	GTGGAGGAAGCCGACAACAATGA
	CAAGCTGATTGGCGATGTGAG
Sox2	TTTTCTAGTCGGCATCACCG
	ACAAGAGAATTGGGAGGGGT
Klf4	GTGCAGCTTGCAGCAGTAAC
	AGCGAGTTGGAAAGGATAAAGTC
Rex1	CAGTCCAGAATACCAGAGTGGAA
	ACTCTAGGTATCCGTCAGGGAAG
Fgfr2	CCCTGCGGAGACAGGTAACAG
	AGCGTCAGCTTATCTCTGGGGA
Fgfr1	ACCCTGTAGCTCCCTACTGGAC
	TGGCATAGCGAACCTTGTAGCC
Fgf4	ACACGAGGGACAGTCTTCTGGA
	TAGGCGTTGTAGTTGTTGGGCA
Fgfbp1	CTAACCTCAAGCTGGTGAACCCC
	TCTCTAATGGCCATGGTCTGGGT
Gapdh	CAACGGCACAGTCAAGGCCGA
	CCCTTCAAGTGGGCCCCGG
Spry2	CCACCGATTGCTTGGAAGTTGG
	AGGTCTTGGCAGTGTGTTCACC
Pre-*Nanog-1*	AGCCCAGTACTCAGGCTTGT
	AGCATCACAACACGCACCT
Pre-*Nanog-2*	GCCAGCAGATGGCATAATTT
	TGATGGCAATGCTGAGGTTA
Pre-*Oct4*	GTCCCAGCTGGTGTGACTCT
	TCTTCTGCTTCAGCAGCTTG
Pre-*Fgf4*	GACTACCTGCTGGGCCTCAAAA
	TACTCAGCCCCCGAGACTACTAC
Pre-*Fgfr2*	CCCGTCCCTTCCCAAATCTGATA
	TCACCTTGGGTCAGGATAACAAG
Pre-*Fgfbp1*	GACTACCTGCTGGGCCTCAAAA
	TACTCAGCCCCCGAGACTACTAC
Pre-*Fgfr1*	CCCGTCCCTTCCCAAATCTGATA
	TCACCTTGGGTCAGGATAACAAG
q-ChIP-PCR primers	
Nanog 5.5 kb	GTGGGTGCACACAGAGAACAAC
	CTGAGAGCTCAGGCCCACAAAG
Nanog -4.9 kb	AACATTCCTTTCCCCACCCACA
	AAGAGGTGGCTGGTAGCCAAAA

Nanog -4.7 kb	TGGGGTAAACTTAAGGCTATGG
	AGCTCTAAGCCGGTTCTCATTT
Nanog -3.9 kb	CCCTACCTCTCCTGAGGTGTGA
	CATGCCTGAGGAAGTCAGAGGA
Nanog -3.4 kb	TGTAGCCCTTGGTTAGTCCGAG
	GGCAGGCATCACCAAAGTCATT
Nanog -1.9 kb	GGTTCAGTCAGGCTGGGCAAT
	CTGCTGCCACACTATCACTGTC
Nanog -1.0 kb	AGCCGACTTAAGCTGGGTTAGA
	TGCTCTAGCTGGTCCCAAACTC
Nanog -0.05 kb	TAGGGTAGGAGGCTTGAGGGG
	AAGTCAGAAGGAAGTGAGCCGC
Nanog +.5 kb	CCGGTGATACGTTGGCCTTCTA
	ACTGCCCCCGAACATATTCCAA
Nanog +1.4 kb	GTTAGGAATGAACGGGTGGGGA
	AGTAGACAGCCCTGAAAGCAGC
Fgf4 +3.5 kb	GCCCAGAACCCAATTTTTATGCAC
	CAAAGTCCCAGAGCCATTCCCTT
Fgf4 -3.0 kb	TTAGCTCGCTTCAGGGAATGCTT
	TTGCTGTCTGTAGCCTCCCATAA
Fgf4 -6.5 kb	CACAAAGGTCGCTTAAGTGGTGG
	ACACGATTTCCAGACTCCTCCAG
Fgf4 -6.9 kb	TTAGGCACCCAAAGGCAGAATTG
	GTCCTGTTATTCATGGCAGGGGA
Fgfr1-5kb	TGGCCTTGGATGAATTGTTGGC
	TTCCACCTCCCTTCAGGACACT
Fgfr1+2.5 kb	TGGGGTGGTGTCTCTTCCTTTCAG
	CAAGCCATTAGGGAGGGAGGCAA
Fgfbp1-1.4 kb	TCCAGTGTGTGTGGTAAACAGGT
	AACACTGCCTCTGGATGGTCTAC
Fgfr2 -2.5 kb	TTTTGTCCCACTTCTTGGGGC
	AATCTTCCACCAGCCTGGACTC
Fgfr2 -4.4 kb	AAACAACGTAACGCATCCACTGT
	TGCACAGATGACCTCTCGGAAC